Mechanisms of Lymphoma Clearance Induced by High-Dose Alkylating Agents

Chen Lossos[1], Yunpeng Liu[2,3], Kellie E. Kolb[2,4,5], Amanda L. Christie[1], Alexandria Van Scoyk[1], Sanjay M. Prakadan[2,4,5], Kay Shigemori[1], Kristen E. Stevenson[1], Sara Morrow[1], Olivia D. Plana[1], Cameron Fraser[6,7], Kristen L. Jones[1], Huiyun Liu[1], Christian P. Pallasch[8], Rebecca Modiste[9], Quang-De Nguyen[9], Jeffrey W. Craig[10], Elizabeth A. Morgan[10], Francisco Vega[11,12], Jon C. Aster[10], Kristopher A. Sarosiek[6,7], Alex K. Shalek[2,4,5], Michael T. Hemann[2,3], and David M. Weinstock[1,2]

ABSTRACT

The extraordinary activity of high-dose cyclophosphamide against some high-grade lymphomas was described nearly 60 years ago. Here we address mechanisms that mediate cyclophosphamide activity in bona fide human double-hit lymphoma. We show that antibody resistance within the bone marrow (BM) is not present upon early engraftment but develops during lymphoma progression. This resistance required a high tumor:macrophage ratio, was recapitulated in spleen by partial macrophage depletion, and was overcome by multiple, high-dose alkylating agents. Cyclophosphamide induced endoplasmic reticulum (ER) stress in BM-resident lymphoma cells *in vivo* that resulted in ATF4-mediated paracrine secretion of VEGFA, massive macrophage infiltration, and clearance of alemtuzumab-opsonized cells. BM macrophages isolated after cyclophosphamide treatment had increased phagocytic capacity that was reversed by VEGFA blockade or SYK inhibition. Single-cell RNA sequencing of these macrophages identified a "super-phagocytic" subset that expressed CD36/FCGR4. Together, these findings define a novel mechanism through which high-dose alkylating agents promote macrophage-dependent lymphoma clearance.

SIGNIFICANCE: mAbs are effective against only a small subset of cancers. Herein, we recapitulate compartment-specific antibody resistance and define an ER stress–dependent mechanism induced by high-dose alkylating agents that promotes phagocytosis of opsonized tumor cells. This approach induces synergistic effects with mAbs and merits testing across additional tumor types.

See related commentary by Duval and De Palma, p. 834.

[1]Department of Medical Oncology, Dana-Farber Cancer Institute and Harvard Medical School, Boston, Massachusetts. [2]Broad Institute of MIT and Harvard University, Cambridge, Massachusetts. [3]MIT Koch Institute for Integrative Cancer Research, Cambridge, Massachusetts. [4]Institute for Medical Engineering and Science (IMES), Department of Chemistry, and Koch Institute for Integrative Cancer Research, MIT, Cambridge, Massachusetts. [5]Ragon Institute of MGH, MIT, and Harvard, Cambridge, Massachusetts. [6]John B. Little Center for Radiation Sciences, Department of Environmental Health, Harvard T.H. Chan School of Public Health, Boston, Massachusetts. [7]Laboratory of Systems Pharmacology, Harvard Program in Therapeutic Science, Department of Systems Biology, Harvard Medical School, Boston, Massachusetts. [8]Department of Internal Medicine, University Hospital of Cologne, Cologne, Germany. [9]Lurie Family Imaging Center, Center for Biomedical Imaging in Oncology, Dana-Farber Cancer Institute, Boston, Massachusetts. [10]Department of Pathology, Brigham and Women's Hospital, Harvard Medical School, Boston, Massachusetts. [11]Division of Hematopathology, Department of Pathology and Laboratory Medicine, University of Miami/Sylvester Comprehensive Cancer Center, Miami, Florida. [12]Division of Hematology-Oncology, Department of Medicine, Sylvester Comprehensive Cancer Center, University of Miami, Miami, Florida.

Note: Supplementary data for this article are available at Cancer Discovery Online (http://cancerdiscovery.aacrjournals.org/).

Corresponding Author: David M. Weinstock, Dana-Farber Cancer Institute, 450 Brookline Avenue, Dana 510B, Boston, MA 02215. Phone: 617-632-4245; Fax: 617-632-6380; E-mail: davidm_weinstock@dfci.harvard.edu

Cancer Discov 2019;9:944–61

doi: 10.1158/2159-8290.CD-18-1393

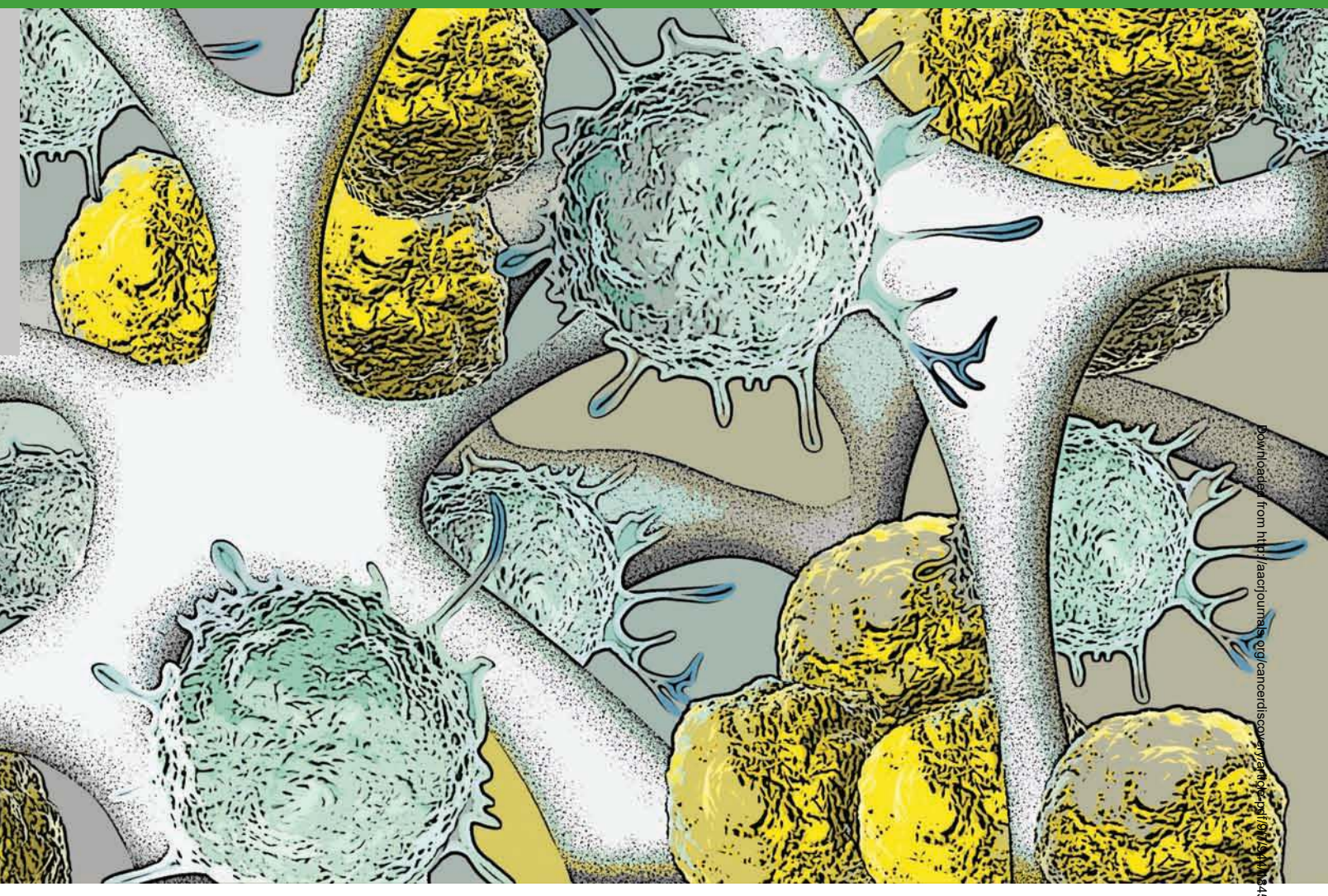

INTRODUCTION

The alkylating agent cyclophosphamide first became available in 1959 (1, 2). Soon after, cyclophosphamide was noted to have remarkable single-agent activity in the treatment of endemic Burkitt lymphoma. In fact, a fraction of high-grade lymphomas could be cured with a single dose of cyclophosphamide (3, 4), a response that is wholly unique among aggressive cancers. The mechanisms through which cyclophosphamide exerts this profound efficacy have remained largely unclear.

Cell lines developed from high-grade lymphomas like Burkitt lymphoma have similar sensitivities to alkylating agents as they do to topoisomerase II poisons (e.g., doxorubicin, etoposide), vinca alkaloids, and other chemotherapies (5–7). Thus, there does not appear to be a lymphoma cell–autonomous sensitivity specific to alkylating agents. This leaves the remarkable *in vivo* activity of high-dose cyclophosphamide unexplained, but one possibility is that it involves the lymphoma microenvironment. High doses of cyclophosphamide are extremely lymphodepleting (8, 9), so it is unlikely that adaptive immunity plays a large role in its activity. In contrast, macrophages are largely resistant to chemotherapy, including high doses of alkylating agents like cyclophosphamide. Chemotherapies such as doxorubicin and cyclophosphamide can be "immunogenic" and increase macrophage-mediated clearance of tumor cells (10, 11). Of note, Burkitt lymphoma and other high-grade lymphomas with *MYC* rearrangements commonly have a "starry sky" appearance under the microscope due to infiltration of the microenvironment by lymphoma-associated macrophages (12, 13).

mAbs like rituximab and alemtuzumab, which bind to CD20 and CD52, respectively, are widely utilized in the treatment of lymphomas. These antibodies function through various mechanisms, including antibody-dependent cellular phagocytosis (ADCP) by macrophages, antibody-dependent cellular cytotoxicity (ADCC) by natural killer cells, and complement-dependent cytotoxicity (CDC; refs. 14–16). Both rituximab and alemtuzumab have reduced activity at sites of bulky disease (17, 18), suggesting at least two possibilities: (i) the antibodies have poor penetration into sites of bulky disease and/or (ii) bulky disease represents a later stage of disease progression, in which the lymphoma microenvironment is less amenable to antibody-dependent lymphoma killing.

We previously treated NOD.SCID.*IL2Rγ*$^{-/-}$ (NSG) mice transplanted with a humanized model of CD20^{lo}CD52^{hi} B-cell leukemia/lymphoma (19) with alemtuzumab, which led to near-elimination of tumor in blood and spleen, but not bone marrow (BM). Resistance in the BM was successfully overcome by treatment with high-dose cyclophosphamide (20). To more faithfully model human aggressive lymphomas, we have established patient-derived xenografts (PDX) of double-hit lymphoma (DHL). DHL is a highly aggressive subtype of B-cell lymphoma that is frequently resistant to rituximab-containing immunochemotherapy like R-CHOP, commonly involves the BM (21, 22), and has a very poor prognosis (23, 24). Novel treatments for DHL are a recognized area of clinical need. Approximately 75% of DHLs highly express CD52, suggesting alemtuzumab may have efficacy in this disease (21). Of note, alemtuzumab has been used extensively to treat chronic lymphocytic leukemia and other lymphoid malignancies involving the BM, especially in the rituximab-refractory setting (25).

Important biological questions from our previous work remain unanswered. First, do the effects of high-dose cyclophosphamide extend to bona fide human lymphomas? Second, do other alkylating agents recapitulate the effects observed with high-dose cyclophosphamide? Third, what components of BM remodeling that occur during disease progression drive therapeutic resistance? Fourth, are macrophages required for cyclophosphamide-mediated killing in the BM microenvironment? Fifth, how does cyclophosphamide induce cross-talk *in vivo* between lymphoma cells and macrophages? Finally, does the *in vivo* cross-talk modify the transcriptional and phenotypic states of macrophages to promote phagocytosis? Here we utilize *in vivo* models of human DHL to specifically address mechanisms underlying the notable activity of high-dose cyclophosphamide described in patients with aggressive lymphomas.

RESULTS

Alkylating Agents Overcome Therapeutic Resistance of Human Lymphoma Cells in the BM

DFBL-20954 and DFBL-69487 are DHL PDXs that harbor translocations of both *MYC* and *BCL2* (Supplementary Fig. S1A; ref. 26). Both DFBL-20954 and DFBL-69487 are CD52^{hi}/CD20$^{lo/negative}$ (Fig. 1A; Supplementary Fig. S1B), consistent with a subset of DHLs (27, 28) and observed with acquired resistance to rituximab-based therapy (29). In fact, both PDXs were established from biopsies obtained after treatment failure with R-CHOP, which includes rituximab and a lower dose of cyclophosphamide (750 mg/m^2).

NSG mice were xenografted with these lymphomas and monitored until they had >2% peripheral blood hCD19$^+$CD45$^+$ cells (approximately days 21 and 35 post-injection for DFBL-20954 and DFBL-69487, respectively). Mice were randomized to receive vehicle, cyclophosphamide (100 mg/kg) on day 0, alemtuzumab (5 mg/kg/day) on days 0 and 1, or the combination (20). Mice treated with alemtuzumab and sacrificed on day 8 had near-complete elimination of lymphoma cells in the peripheral blood and spleen compared with vehicle-treated mice, but alemtuzumab had almost no effect in the BM (Fig. 1B and C; Supplementary Fig. S2A). *In vitro* exposure to alemtuzumab for 48 hours had no effect on the viability of either PDX (Supplementary Fig. S2B), suggesting that alemtuzumab efficacy is dependent on *in vivo* factors.

Lower doses of cyclophosphamide (25 or 50 mg/kg) had markedly reduced effects on BM DHL cells compared with cyclophosphamide 100 mg/kg (Supplementary Fig. S2C). Consistent with low expression of CD20 on both DHLs, rituximab failed to synergize with high-dose cyclophosphamide in eliminating splenic and BM disease (Supplementary Fig. S2D). Moreover, high-dose cyclophosphamide and alemtuzumab induced significantly greater BM tumor clearance than an R-CHOP regimen (30, 31). Rituximab failed to induce apoptosis or phagocytosis by BM-derived macrophages (BMDM) *in vitro* (Supplementary Fig. S2E and S2F).

Treatment with the MTD of doxorubicin also reduced splenic, but not BM, lymphoma, and was not synergistic with alemtuzumab (Fig. 1B). Because doxorubicin induces DNA double-strand breaks (DSB) that lead to apoptosis, we hypothesized that lymphoma cells resident within the BM may be less susceptible to DNA damage–induced apoptosis (i.e., less "primed") than those in the spleen. We used BH3 profiling (32) to assess apoptotic priming of lymphoma cells from the two compartments, which involves adding proapoptotic peptides to cells and quantifying the extent to which they induce mitochondrial permeabilization. Surprisingly, BM lymphoma cells were more primed to undergo apoptosis than spleen lymphoma cells (Supplementary Fig. S2G). Thus, the resistance of BM lymphoma cells to doxorubicin involves non-lymphoma cell–autonomous effects within the BM microenvironment.

In contrast to doxorubicin, cyclophosphamide monotherapy reduced lymphoma burden by approximately 10-fold in the BM and was highly synergistic (160-fold in DFBL-20954, 88-fold in DFBL-69487) with alemtuzumab (Fig. 1B). Importantly,

Figure 1. Alkylating agents overcome bone marrow antibody resistance. **A,** Flow cytometric analysis of surface CD20 and CD52 expression on DFBL-20954 and DFBL-69487. **B,** On day 8 of treatment, spleen was harvested and a single femur was flushed from mice treated with PBS, cyclophosphamide (CTX), doxorubicin (Dox), alemtuzumab (Alem), or combinations, as indicated. Total cells were counted and analyzed for the indicated markers. Total tumor cells present are represented as the product of total cells * viable (7-AAD$^-$) hCD19/hCD45 double-positive cells. All comparisons by two-sided Welch test, *, $P < 0.05$; **, $P < 0.01$; ***, $P < 0.001$. **C,** ^{18}FDG-PET imaging of mice engrafted with DFBL-20954 at day 21 post-injection (left) and 48 hours after alemtuzumab (Alem) treatment (right) shows progression of disease in bone marrow (e.g., femurs and tibia) but resolution of disease in lymph node regions (e.g., in the axillae). **D,** Kaplan–Meier curves of overall survival of NSG mice engrafted with DFBL-20954 and DFBL-69487 treated with PBS, cyclophosphamide, alemtuzumab, or cyclophosphamide + alemtuzumab. $P < 0.0001$ cyclophosphamide versus Veh, $P < 0.001$ cyclophosphamide + alemtuzumab versus cyclophosphamide for 20954, $P < 0.001$ cyclophosphamide + alemtuzumab versus cyclophosphamide for 69487, $P < 0.001$ for cyclophosphamide + alemtuzumab versus cyclophosphamide for both. All comparisons by log-rank test. **E,** Bone marrow tumor burden of NSG mice engrafted with DFBL-20954 and treated with PBS, alemtuzumab, cyclophosphamide, ifosfamide (ifos), busulfan (bu), or navitoclax. Total tumor burden was assessed from one femur as in **B**. All comparisons by two-sided Welch *t* test.

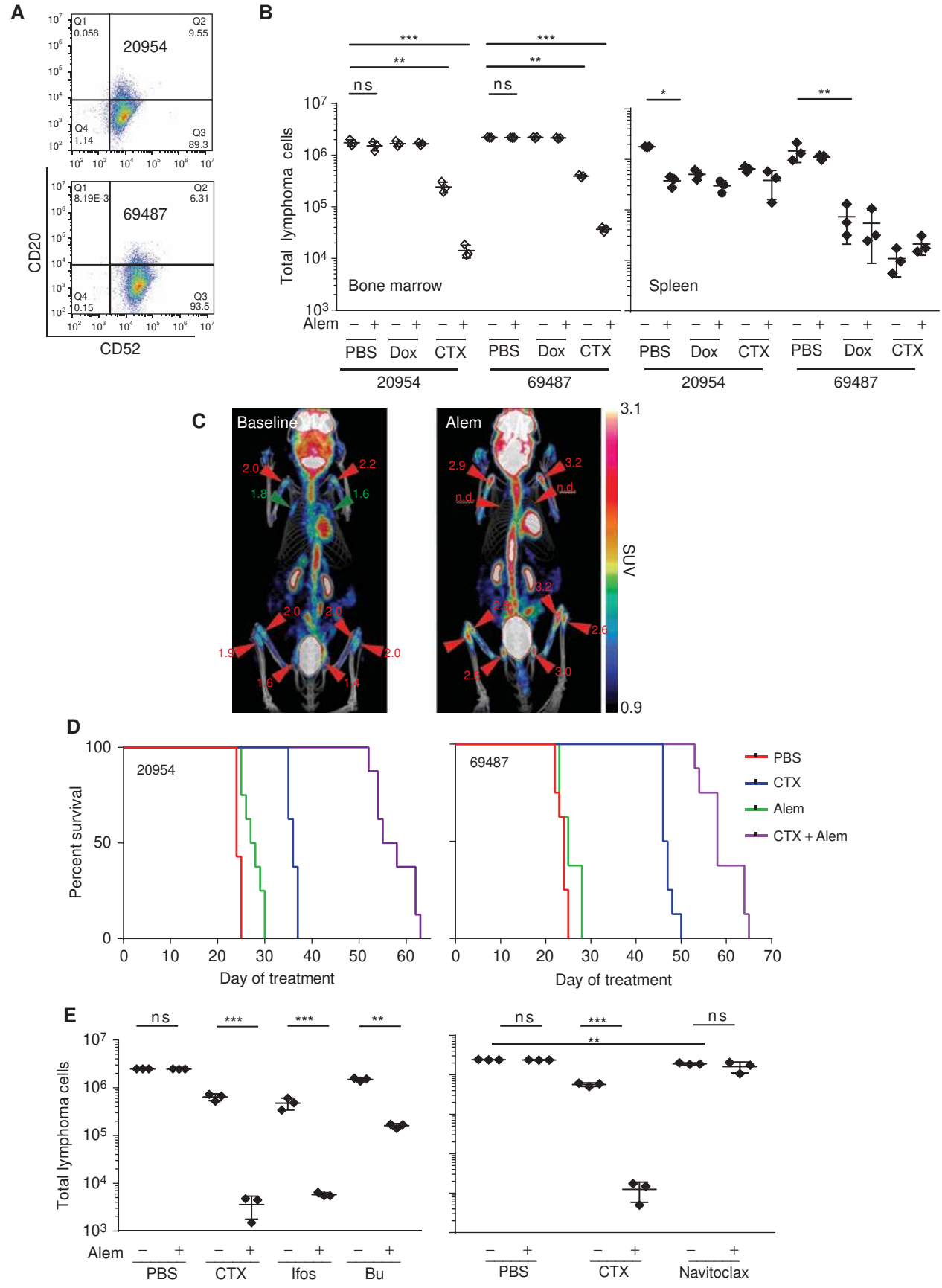

in vivo treatment with doxorubicin or cyclophosphamide induced similar levels of DNA DSBs (Supplementary Fig. S2H) and apoptotic priming (Supplementary Fig. S2I) within BM lymphoma cells. Thus, the unique efficacy of cyclophosphamide is unlikely to depend solely on DNA damage or induction of lymphoma apoptosis. Treatment with cyclophosphamide resulted in significantly increased survival compared with vehicle- or alemtuzumab-treated mice ($P < 0.001$; Fig. 1D). Mice receiving the combination of cyclophosphamide plus alemtuzumab had significantly increased survival compared with either agent alone (both comparisons $P < 0.001$; Fig. 1D), consistent with *in vivo* synergy.

We next asked whether other alkylating agents could recapitulate the effects of cyclophosphamide on lymphoma cells in the BM. Like cyclophosphamide, the nitrogen mustard ifosfamide and the alkyl sulfonate busulfan each reduced lymphoma burden in the BM of treated mice and were synergistic with alemtuzumab (Fig. 1E). The BCL2/BCL-xL inhibitor navitoclax reduced BM lymphoma percentage by approximately 20% ($P = 0.0011$ vs. PBS) but, in contrast with the alkylating agents, did not induce synergistic effects with alemtuzumab (Fig. 1E). Thus, synergy with alemtuzumab is unlikely to depend solely on the induction of apoptosis.

Lymphoma:Effector Ratio Determines the Response to Alemtuzumab

To address the mechanisms of alemtuzumab resistance in the BM, we first asked whether the burden of disease affected therapeutic efficacy. We injected DFBL-20954 cells into mice and initiated alemtuzumab treatment after 8, 12, or 16 days. Treatment with alemtuzumab at any of the time points led to marked reductions in spleen lymphoma cells 3 days after treatment initiation (e.g., at day 11 after treatment on day 8; Fig. 2A). In contrast, alemtuzumab reduced BM lymphoma cells when given on days 8 or 12 but not when given on day 16 (Fig. 2A) or 21 (Fig. 1C). Thus, resistance to alemtuzumab in the BM is associated with more extensive lymphoma involvement. Alemtuzumab labeling of lymphoma cells was similar in the BM and spleen of mice treated 21 days after xenografting (Fig. 2B). Moreover, alemtuzumab binding of lymphoma cells was detected in the BM up to 5 days after dosing (Supplementary Fig. S3A), consistent with past reports of alemtuzumab *in vivo* half-life (33, 34). Together, these data suggest that resistance to alemtuzumab within the BM is not due to inadequate antibody penetration.

We next asked whether resistance was driven by differences in macrophage involvement between the BM and spleen. We treated lymphoma-engrafted mice with clodronate at a dose that almost completely depleted macrophages from the spleen and BM (Supplementary Fig. S3B). We dosed alemtuzumab on day 12 after xenografting, a timepoint when alemtuzumab leads to approximately 50% depletion of BM lymphoma cells 3 days later (Fig. 2A). Treatment with clodronate on day 10 (2 days prior to alemtuzumab) completely abrogated alemtuzumab effects in both the spleen and BM (Fig. 2C). Thus, macrophages are required for alemtuzumab-mediated lymphoma clearance. Pretreatment with clodronate also largely reversed the effects of cyclophosphamide (alone or with alemtuzumab) on lymphoma involvement in the BM (Fig. 2D), indicating that macrophages contribute to cyclophosphamide-induced lymphoma clearance.

We next asked whether lymphoma engraftment within the BM reduces the phagocytic capacity of macrophages within that compartment. We sorted primary CD11b$^+$F4/80$^+$ monocytes/macrophages from the BM of either unengrafted NSG mice or NSG mice bearing the lymphoma xenografts. We then assayed *ex vivo* phagocytosis of BM lymphoma cells collected from untreated mice. *Ex vivo* phagocytosis did not differ significantly between macrophages from BM of unengrafted NSG mice and from NSG mice engrafted with lymphoma on day 21, either in the presence or the absence of alemtuzumab (Fig. 2E). The same results were observed using the Burkitt lymphoma cell line Raji, to which the macrophages were not previously exposed (Fig. 2E). These data suggest that "tolerization" of macrophages induced by lymphoma cells was not a driver of BM resistance.

We next asked whether BM resistance to alemtuzumab at day 21 was due to an inherently lower phagocytic capacity of BM macrophages to phagocytose lymphoma cells compared

Figure 2. BM resistance to alemtuzumab (Alem) involves microenvironmental remodeling. **A,** 1×10^6 DFBL-20954 cells were injected into NSG mice, and alemtuzumab treatment (daily × 2) was initiated on the indicated days 8, 12, and 16 (base of blue arrows). The tips of the blue arrows correspond to tumor burden of mice treated with alemtuzumab at 48 hours after the second treatment dose. $N = 3$ mice for each condition at each time point. **B,** Assessment of DFBL-20954 lymphoma cells after *in vivo* treatment with APC-conjugated alemtuzumab. Representative flow cytometry plots shown. **C,** On day 10 after transplant of 1×10^6 DFBL-20954 cells, mice were treated with clodronate liposomes (clod, 200 μL) or PBS. Alemtuzumab was given as a single dose of 10 mg/kg i.v. on day 12. Tumor burden was assessed 48 hours after treatment. Two-sided Welch *t* test, *, $P < 0.05$; **, $P < 0.01$; ***, $P < 0.001$. **D,** On day 19 after transplant of 10^6 DFBL-20954 cells, mice received clodronate or PBS (−). On day 21, mice received cyclophosphamide, alemtuzumab (10 mg/kg i.v. single dose), the combination, or vehicle (PBS) and assessed for tumor burden on day 23. Mouse cells were depleted and human cell numbers and viability were assessed with Trypan blue staining. Tumor burden is reported as the number of viable tumor cells. Two-sided Welch *t* test. **E,** Primary, viable BM (7-AAD$^-$hCD19$^-$CD11b$^+$F4/80$^+$) monocytes/macrophages were sorted from unengrafted or lymphoma-engrafted NSG mice. BM tumor cells from corresponding engrafted mice or Raji cells were incubated in the presence or absence of alemtuzumab. All comparisons between unengrafted and vehicle under the same conditions ($n = 3$ per condition) were nonsignificant. **F,** Primary viable splenic (7AAD$^-$hCD19$^-$CD11b$^-$F4/80$^+$) and BM (7AAD$^-$hCD19$^-$CD11b$^+$F4/80$^+$) monocytes/macrophages were sorted from unengrafted or lymphoma-engrafted NSG mice and cultured with BM lymphoma cells from the corresponding xenograft that were treated *ex vivo* with alemtuzumab. All comparisons between splenic and BM macrophages under the same conditions ($n = 3$ per condition) were nonsignificant. **G,** Ratio of lymphoma to macrophage cells 48 hours after chemotherapy initiation of DFBL-20954–engrafted mice. Two-sided Welch *t* test, *, $P < 0.05$. Doxorubicin versus cyclophosphamide (CTX) BM not significant. **H,** Mice were engrafted with DFBL-20954 and given clodronate (25 μL) or vehicle on day 19 followed by alemtuzumab or vehicle on day 21 and 22 and then sacrificed 48 hours after dosing. Spleen tumor burden shown. Two-sided Welch *t* test, *, $P < 0.05$; **, $P < 0.01$; ***, $P < 0.001$. **I,** Macrophage BM (hCD19$^-$CD11b$^+$F4/80$^+$) cellularity based on flow cytometry 8 days after initiation of the indicated agents. Two-sided Welch *t* test, *, $P < 0.05$; **, $P < 0.01$; ***, $P < 0.001$. Comparison of PBS versus cyclophosphamide shown for both xenografts. Cyclophosphamide versus doxorubicin across all conditions significant ($P < 0.001$ for DFBL-20954 and $P < 0.05$ for DFBL-69487). **J,** Representative anti-F4/80 staining (brown) of fixed femurs from mice engrafted with DFBL-20954 or DFBL-69487 and harvested 40 hours after treatment with the indicated agents. Images are 1× and 20× magnified as indicated.

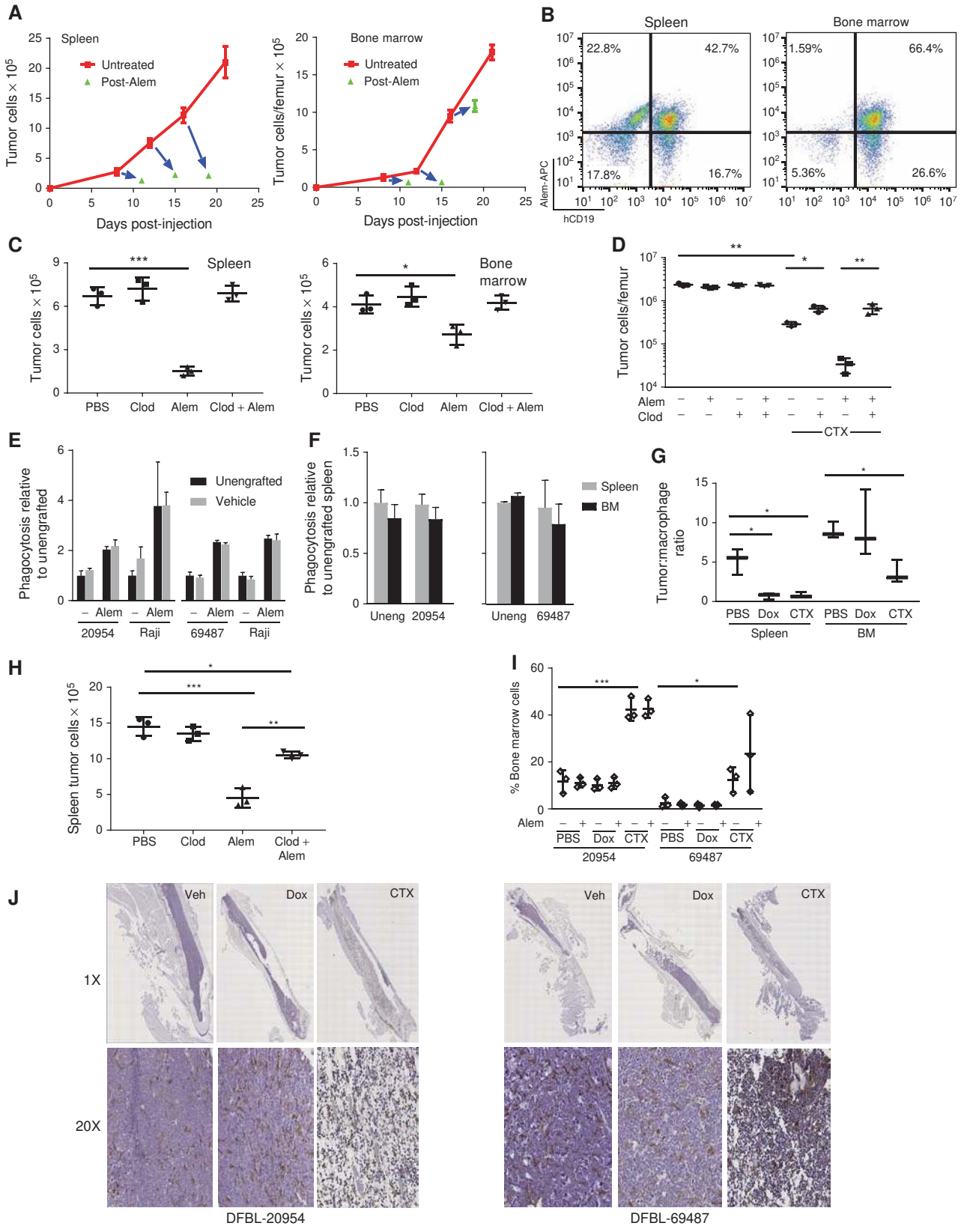

with spleen macrophages. To test this, we sorted splenic and BM macrophages from unengrafted NSG mice or mice engrafted with lymphoma on day 21 and assayed their *ex vivo* capacity to phagocytose BM lymphoma cells. Again, there were no differences in the phagocytic capacity of splenic and BM macrophages *ex vivo* (Fig. 2F).

We noted that at day 21 after xenografting, mice had 2-fold (model 20954; Fig. 2G) or 8-fold (model 69487; Supplementary Fig. S3C) higher lymphoma:macrophage (i.e., target:effector) ratios in the BM compared with the spleen. To more rigorously assess whether the lymphoma:macrophage ratio was a driver of antibody resistance, we gave a reduced dose of clodronate to lymphoma-engrafted mice to partially deplete macrophages and thereby establish a lymphoma:macrophage ratio in the spleen like that observed in the BM. At a dose of clodronate that reduced splenic macrophages by approximately 75% (Supplementary Fig. S3D), the effects of alemtuzumab on splenic lymphoma were almost completely reversed (Fig. 2H). Together, these data suggest that the higher lymphoma:macrophage ratio that occurs upon extensive BM lymphoma involvement is the primary driver of alemtuzumab resistance.

Treatment with cyclophosphamide but not doxorubicin significantly reduced the BM lymphoma:macrophage ratio in both models (Fig. 2G; Supplementary Fig. S3C). This was associated with a striking increase in the fractional abundance of macrophages in the BM 8 days after treatment with cyclophosphamide but not with doxorubicin (Fig. 2I). Because macrophages can adhere to stromal elements within the BM microenvironment and be difficult to remove by mechanical flushing, flow cytometric quantification may underestimate macrophage involvement. Thus, we stained femurs from treated mice for the macrophage marker F4/80, which showed that the BM space of cyclophosphamide-treated mice was packed with macrophages (Fig. 2J). Fewer than 5% of macrophages within the BM of cyclophosphamide-treated mice were in the S or G_2–M phase of the cell cycle (Supplementary Fig. S3E), suggesting that these cells did not proliferate within the BM but instead trafficked there after cyclophosphamide treatment.

Reduced Phagocytic Proneness of BM Lymphoma Cells Is Reversed by Cyclophosphamide

Having established that lymphoma:macrophage ratios differ within the BM and spleen at late timepoints, we next asked whether the altered ratio could be due to BM lymphoma cells being less prone to macrophage phagocytosis. We isolated viable (Annexin V–negative) lymphoma cells from the spleen and BM 21 days after xenografting and assessed their capacity to be phagocytosed by BMDMs from unengrafted NSG mice *ex vivo* (see Methods). More splenic lymphoma cells were phagocytosed compared with BM lymphoma cells, in both the presence and absence of alemtuzumab (Fig. 3A). In addition, more BM lymphoma cells from mice treated with cyclophosphamide were phagocytosed compared with lymphoma cells from mice treated with vehicle or doxorubicin (Fig. 3A).

To address the mechanisms underlying reduced macrophage phagocytosis of BM lymphoma cells, we quantified levels of factors known to affect phagocytosis or antibody efficacy at day 21 after xenografting. We identified increased levels of the antiphagocytic factors prostaglandin E2 (PGE2; ref. 35), CD32 (36), and galectin-1 (37) in BM lymphoma cells compared with spleen lymphoma cells (Fig. 3B). At the same time, the prophagocytic molecule VSIR (38) was decreased in BM lymphoma cells compared with spleen lymphoma cells (Fig. 3B). The addition of recombinant PGE2 (2 ng/mL) inhibited macrophage phagocytosis of BM lymphoma cells *in vitro* in both the presence and absence of alemtuzumab (Fig. 3C; Supplementary Fig. S4A). Similarly, the addition of recombinant galectin-1 (500 ng/mL) inhibited antibody-mediated phagocytosis of lymphoma cells by BMDMs *ex vivo*, which was reversed by the galectin-1 inhibitor lactose (Fig. 3D).

We hypothesized that cyclophosphamide augments lymphoma cell phagocytic proneness by shifting the balance of pro- and antiphagocytic factors. Indeed, treatment with cyclophosphamide lowered surface levels of the antiphagocytic molecule CD47 and increased surface expression of both VSIR and calreticulin (Fig. 3E; Supplementary Fig. S4B). In contrast, cyclophosphamide had no effect on the levels of surface CD52 (Fig. 3E). Total levels of PGE2 and galectin-1 were reduced in lymphoma cells from the BM of cyclophosphamide-treated mice compared with vehicle- or doxorubicin-treated mice (Fig. 3E; Supplementary Fig. S4B). These observations suggest that high-dose cyclophosphamide increases the susceptibility of human lymphoma cells to be phagocytosed by macrophages at least in part through remodeling of effector:target interactions.

To further confirm this model, we generated conditioned media by isolating BM lymphoma cells from mice 21 days after engraftment and 6 hours after *in vivo* treatment with PBS, doxorubicin, or cyclophosphamide. Equal numbers of lymphoma cells from each condition were washed and then incubated *ex vivo* for 24 hours. The conditioned media were then applied to a coculture of NSG BMDMs with lymphoma cells in the presence or absence of alemtuzumab. Conditioned media generated from cyclophosphamide-treated lymphoma cells increased phagocytosis in the presence of alemtuzumab (Fig. 4A), confirming that humoral factors induced by cyclophosphamide treatment can promote ADCP. Human cytokine profiling of whole BM identified increases in both VEGFA and IL16 from mice treated with cyclophosphamide, ifosfamide, or busulfan (Fig. 4B; Supplementary Fig. S4C and S4D). Increased levels of human VEGFA were also observed in the conditioned media from mice treated with cyclophosphamide (Supplementary Fig. S4E). Consistent with the role of IL16 in specifically recruiting $CD4^+$ macrophages (39), we observed a higher fraction of macrophages that were $CD4^+$ in the BM of cyclophosphamide-treated but not doxorubicin-treated mice (Supplementary Fig. S4F).

The addition of recombinant human VEGFA increased *in vitro* phagocytosis of alemtuzumab-treated lymphoma cells by BMDMs (Fig. 4C). Addition of the anti-human VEGFA antibody bevacizumab completely blocked the prophagocytic effect of conditioned media collected from the BM of lymphoma-engrafted mice treated with cyclophosphamide (Fig. 4D). Higher doses of recombinant galectin-1 (1 μg/mL) and PGE2 (5 ng/mL) were needed to inhibit BMDM phagocytosis upon incubation with cyclophosphamide-conditioned media (compared with control media; Fig. 4D), consistent with reductions in their concentrations in the cyclophosphamide-conditioned media (Fig. 3E). Treatment

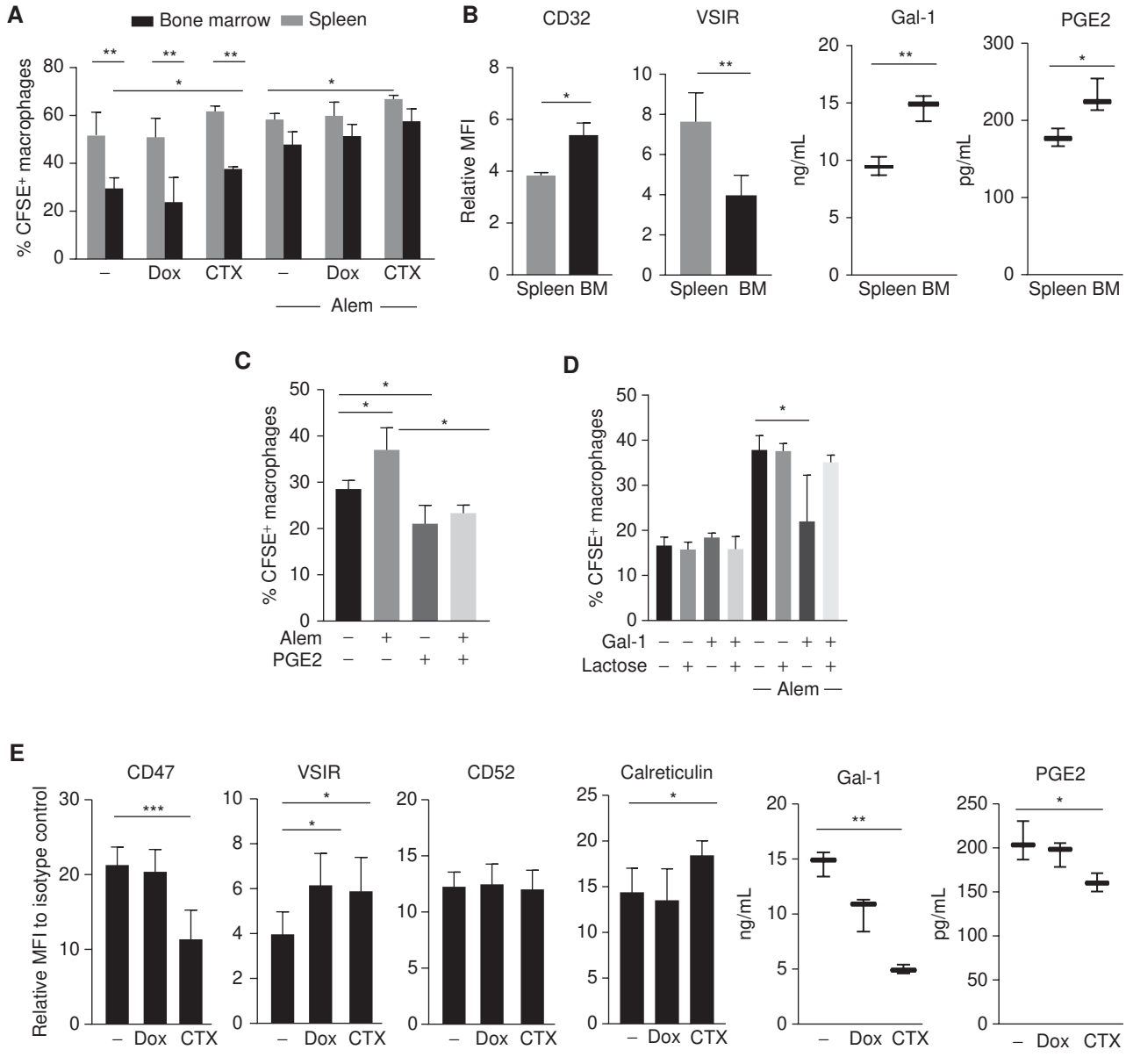

Figure 3. Cyclophosphamide promotes lymphoma phagocytosis by macrophages. **A,** Tumor cells from the spleen and BM of mice ($n = 3$ per condition) engrafted with DFBL-20954 were isolated by mouse cell depletion 16 hours after treatment with PBS, doxorubicin (Dox), or cyclophosphamide (CTX). Dead cells were removed and the remaining live tumor cells were incubated *ex vivo* with BM-derived macrophages in the presence and absence of alemtuzumab (Alem). Two-sided Welch *t*-test, *, $P < 0.05$; **, $P < 0.01$; ***, $P < 0.001$. **B,** Surface expression by mean fluorescence intensity (MFI) compared with isotype control or total protein level by ELISA for the indicated proteins in the bone marrow and spleen of DFBL-20954–engrafted mice ($n = 3$–6 per condition). Paired two-sided *t* test. **C,** DFBL-20954 cells ($N = 3$ mice) were isolated from BM of untreated mice, labeled with CFSE, and cocultured with BM-derived macrophages in the presence or absence of alemtuzumab and prostaglandin E2 (PGE2, 2 ng/mL). Phagocytosis was quantified as percent of CD11b$^+$ cells that were CFSE$^+$. The experiment was performed three times and a representative example is shown. **D,** As in **C** but with recombinant human galectin-1 (Gal-1, 500 ng/mL) and lactose (20 mmol/L). **E,** DFBL-20954–engrafted mice ($n = 3$–6 per condition) were treated with the indicated agents and assayed for surface expression of the indicated markers on viable tumor cells. CD47 and VSIR were quantified at 16 hours post-treatment; CD52 and Calreticulin at 48 hours posttreatment. PGE2 and Gal-1 levels were quantified by ELISA 48 hours posttreatment.

of lymphoma-engrafted mice with bevacizumab decreased the efficacy of cyclophosphamide plus alemtuzumab *in vivo*, confirming that VEGFA secreted by human lymphoma cells in the BM is necessary for maximal synergy (Fig. 4E).

Previous reports have demonstrated that VEGFA increases phosphorylation of the SYK kinase in macrophages, which is also downstream of Fc receptors and known to be essential for antibody-mediated phagocytosis (40). We confirmed that VEGFA increased SYK phosphorylation in BMDMs ($P < 0.05$; Supplementary Fig. S4G). VEGFA also enhanced SYK phosphorylation over levels induced by antibody-Fc cross-linking ($P < 0.05$; Supplementary Fig. S4G). Addition of the SYK inhibitor BAY61-3606 blocked SYK phosphorylation that was induced by VEGFA and

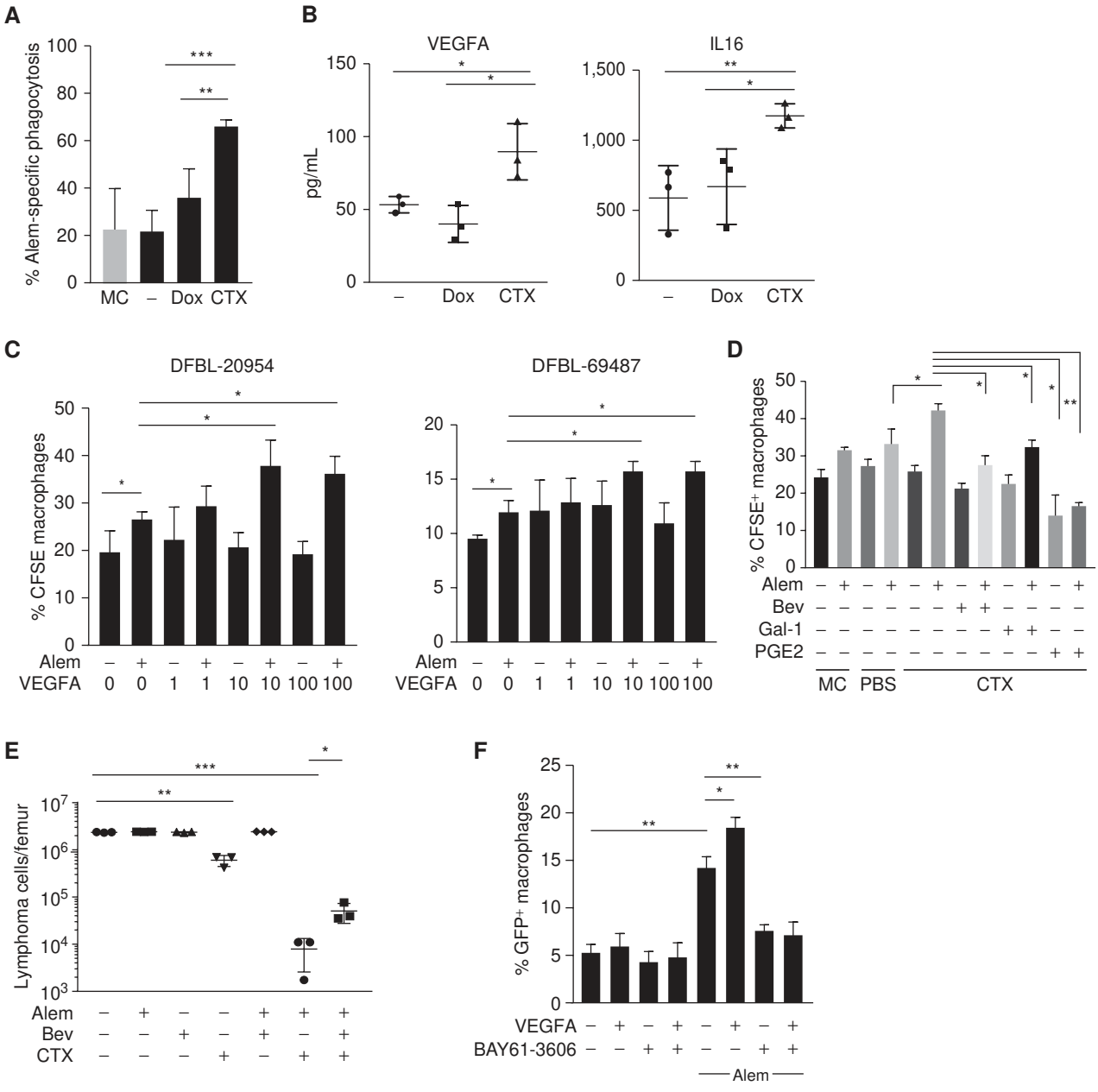

Figure 4. Cyclophosphamide induces DHL secretion of VEGFA and IL16 to promote tumor clearance. **A,** DFBL-20954 cells were isolated from BM of untreated mice, labeled with CFSE, and cocultured with BMDMs and conditioned media from mice ($n = 3$ per condition) treated as indicated. MC, media control. Alemtuzumab-specific killing is defined as the % increase in CFSE$^+$ macrophages in the presence of alemtuzumab compared with no antibody. Unpaired two-sided *t* test, **, $P < 0.01$; ***, $P < 0.001$. **B,** Levels of human VEGFA and IL16 from bone marrow of DFBL-20954–engrafted mice collected 16 hours after *in vivo* treatment with vehicle (–), doxorubicin (Dox), or cyclophosphamide (CTX). Representative experiment shown. Levels of murine VEGFA by the same cytokine arrays were <1 pg/mL. Unpaired two-sided *t* test, *, $P < 0.05$; **, $P < 0.01$. **C,** BMDMs were incubated with CFSE-labeled BM lymphoma cells ($N = 3$ mice) from untreated mice supplemented with alemtuzumab, recombinant human VEGFA, or vehicle (–). Experiments were performed ≥2 times and representative examples are shown. Phagocytosis was assessed as the percent of CD11b$^+$ cells that were CFSE$^+$. Two-sided Welch's *t* test, *, $P < 0.05$. **D,** BMDMs were incubated with CFSE-labeled BM lymphoma cells from untreated mice and conditioned media ($n = 3$ mice per condition) supplemented with vehicle (–), alemtuzumab, recombinant Gal-1 (1 μg/mL), PGE2 (5 ng/mL), and/or bevacizumab (Bev; 30 μg/mL). Unpaired two-sided *t* test. **E,** BM tumor burden of DFBL-20954–engrafted mice on day 8 after treatment with the indicated agents. Two-sided Welch *t* test. **F,** BMDMs were incubated with GFP$^+$ Raji cells and recombinant human VEGFA (10 ng/mL) in the presence and absence of alemtuzumab. The experiment was performed three times and a representative example is shown. The SYK inhibitor BAY61-3606 (20 nmol/L) was added as indicated. Phagocytosis was assessed as the percent of CD11b$^+$ cells that were GFP$^+$. Unpaired two-sided *t* test.

cross-linking (Supplementary Fig. S4G) and abrogated the ability of VEGFA to enhance macrophage phagocytosis of alemtuzumab-treated lymphoma cells *in vitro* (Fig. 4F). Taken together, these studies suggest that VEGFA enhances macrophage phagocytosis through SYK activation and that this effect is reversed by a SYK inhibitor.

Cyclophosphamide Induces a Secretory Response within BM Lymphoma Cells through Endoplasmic Reticulum Stress

We next sought to understand what promotes cyclophosphamide-mediated VEGFA production. We performed RNA-sequencing (RNA-seq) analysis of purified lymphoma cells from the spleen and BM collected 16 hours after vehicle, doxorubicin, or cyclophosphamide treatment. VEGFA mRNA expression was increased after cyclophosphamide but not doxorubicin treatment in both spleen and BM cells (Supplementary Table S1).

We performed gene-set enrichment analyses (GSEA) and focused on signatures that were specifically enriched in lymphoma cells from both the spleen and BM of cyclophosphamide-treated mice compared with PBS- or doxorubicin-treated mice. We noted multiple signatures corresponding to NF-κB activation, amino acid deprivation, and endoplasmic reticulum (ER) stress (Fig. 5A; Supplementary Table S2). Amino acid deprivation is known to activate the ER stress executioner protein ATF4 (41). ER stress can also drive NF-κB activation and VEGFA secretion in multiple contexts (42–45). ATF4 and spliced XBP1 can both induce VEGFA transcription (43, 46, 47) and were increased in BM lymphoma cells from cyclophosphamide-treated mice compared with vehicle- or doxorubicin-treated mice (Fig. 5B; Supplementary Fig. S5A and S5B).

Ex vivo exposure of BM lymphoma cells to either of the ER stress–inducing agents thapsigargin or tunicamycin was sufficient to increase production and secretion of VEGFA (Fig. 5C; Supplementary Fig. S5C). Of note, a lower dose of cyclophosphamide (50 mg/kg) given *in vivo* was unable to induce ATF4 protein or secretion of VEGFA in BM lymphoma cells but did partially induce spliced XBP1 (Fig. 5D and E). ChIP-qPCR of purified BM lymphoma cells demonstrated significantly increased ATF4 recruitment to exon 1 of *VEGFA* (47) after cyclophosphamide treatment, but not to a negative control region (Fig. 5F). We also observed ATF4 recruitment to *VEGFA* following doxorubicin treatment in the DFBL-69487 model, but to a lesser extent than following cyclophosphamide treatment. Together, these observations suggest that high-dose cyclophosphamide induces ER stress within BM lymphoma cells that involves upregulation of ATF4, which drives VEGFA production and secretion.

Cyclophosphamide Treatment of Lymphoma Cells Induces a Prophagocytic Transcriptional Response in BM Macrophages That Synergizes with Alemtuzumab

Next, we addressed the effects of cyclophosphamide treatment on macrophages within the BM lymphoma environment. We isolated BM and splenic macrophages from lymphoma-bearing mice 48 hours after treatment with vehicle, doxorubicin, or cyclophosphamide and assayed their capacity to phagocytose alemtuzumab-coated lymphoma cells. Macrophages were also isolated from unengrafted NSG mice after treatment with vehicle or cyclophosphamide. Phagocytosis of Raji lymphoma cells was similar between macrophages from unengrafted mice treated with vehicle or cyclophosphamide (Fig. 6A; Supplementary Fig. S6A). In contrast, phagocytosis was markedly increased by macrophages from lymphoma-bearing mice after treatment with cyclophosphamide compared with vehicle (Fig. 6A; Supplementary Fig. S6A). Importantly, this effect was not due to nonspecific cell death, as doxorubicin treatment, which induces similar levels of cell death as cyclophosphamide treatment in the spleen (Fig. 1B), did not increase the phagocytic capacity of splenic macrophages from engrafted mice for lymphoma cells (Fig. 6A; Supplementary Fig. S6A). This effect was not specific to alemtuzumab, as macrophages from tumor-bearing, cyclophosphamide-treated mice also had increased uptake of rituximab-coated Raji cells (Supplementary Fig. S6B). High doses of cyclophosphamide (100 mg/kg) were required to enhance phagocytosis of cells coated with either antibody (Supplementary Fig. S6B). In addition, *ex vivo* pretreatment of macrophages with doxorubicin, mafosfamide (a cyclophosphamide analogue that is active *in vitro*), or ifosfamide failed to increase phagocytosis (Supplementary Fig. S6C). These observations indicate that *in vivo* treatment with cyclophosphamide in the presence of lymphoma is required to enhance the phagocytic capacity of macrophages.

To define transcriptional correlates for these phenotypes, we sorted primary BM macrophages 48 hours after *in vivo* treatment of engrafted mice with vehicle, alemtuzumab, doxorubicin, cyclophosphamide, or cyclophosphamide plus alemtuzumab and performed RNA-seq (Supplementary Table S3). The same population was also sorted from the BM of unengrafted NSG mice treated with either vehicle or cyclophosphamide. Macrophages are commonly categorized by transcriptional signatures into M0 (undifferentiated), M1 (antitumor), and M2 (tumor-promoting) subtypes. We performed multidimensional scaling (MDS) analysis using existing signatures from *in vitro*–differentiated M0, M1, and M2 macrophages as reference groups (48). Macrophages from unengrafted NSG mice treated with vehicle clustered farthest from any of the three reference groups. Upon engraftment of lymphoma cells, the macrophages shifted to a more M2-like signature (Fig. 6B) that was unaffected by *in vivo* treatment with alemtuzumab or doxorubicin. Treatment of either unengrafted mice or lymphoma-engrafted mice with cyclophosphamide (or the combination of cyclophosphamide plus alemtuzumab) generated a new transcriptional cluster (Fig. 6B) that was distinct by differential gene expression (Supplementary Fig. S6D; Supplementary Table S4). This new cluster was closer to M2 by MDS but did not differ in surface expression of MHC class II and CD206 compared to BM macrophages from vehicle-, doxorubicin- or alemtuzumab-treated mice (Supplementary Fig. S6E).

Bulk RNA-seq such as the experiments outlined above cannot distinguish whether cyclophosphamide induces a heterogenous mixture of different macrophage types. Therefore, we also performed Smart-Seq2 single-cell RNA-seq (scRNA-seq; ref. 49) on BM macrophages collected 48 hours after treatment of mice engrafted with either lymphoma and treated with vehicle, doxorubicin, or cyclophosphamide, or unengrafted mice treated with vehicle or cyclophosphamide. After filtering for quality (see Supplementary Methods), we

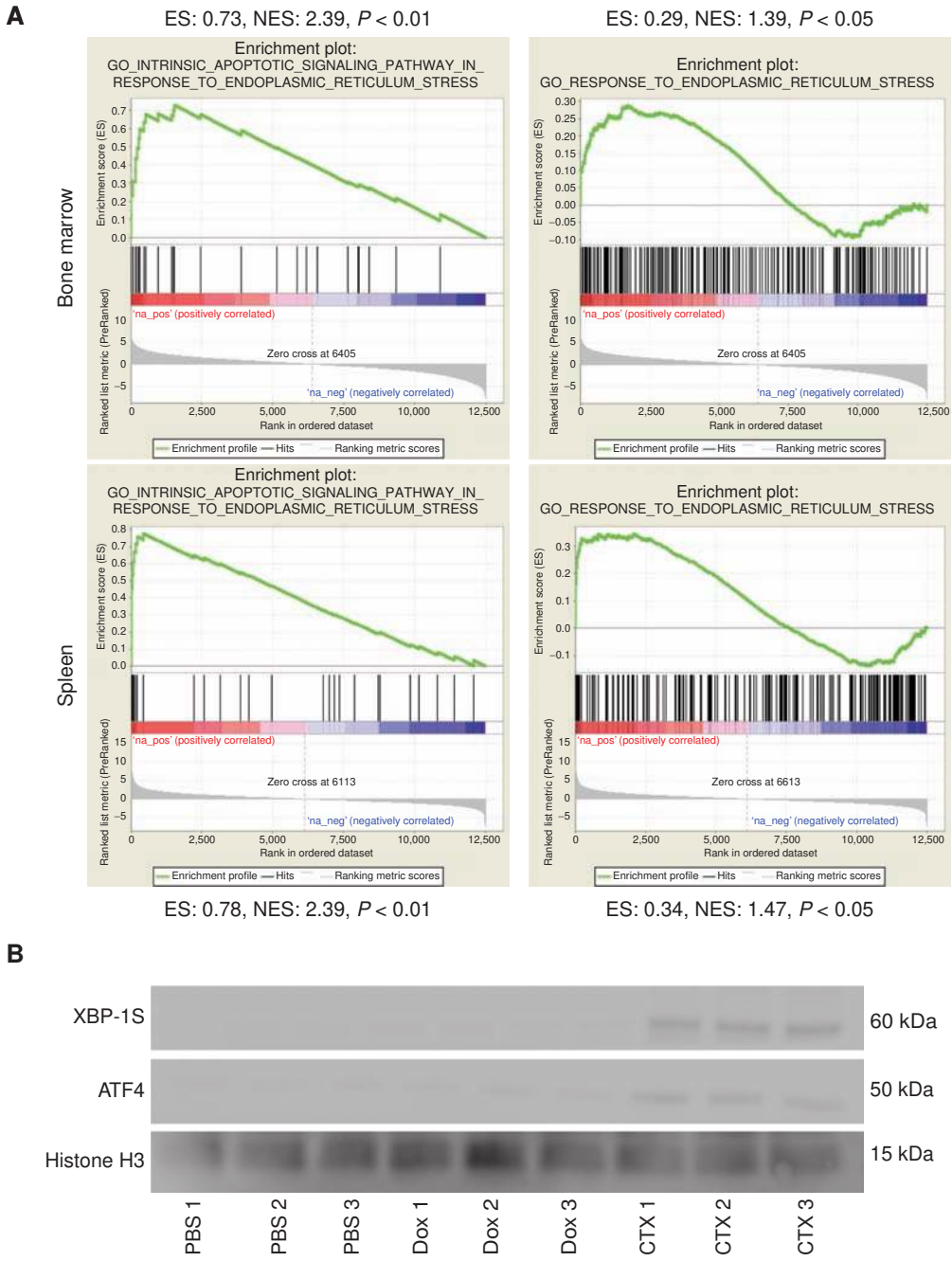

Figure 5. Cyclophosphamide induces ER stress in DHL cells that drives cytokine secretion. **A,** GSEA of ER stress signatures from RNA sequencing of DFBL-20954 cells collected from spleens or BM. The comparison reflects genes that were overexpressed after cyclophosphamide (CTX) treatment as compared with PBS treatment. *P* values have a FDR adjustment. ES, enrichment score; NES, normalized enrichment score. **B,** Immunoblotting for the indicated targets using lysates from purified, viable BM DFBL-20954 cells collected 16 hours after *in vivo* treatment with PBS (vehicle), doxorubicin (Dox), or cyclophosphamide (CTX). Each lane represents an individual mouse. (*continued on following page*)

performed dimensionality reduction (principal component analyisis) and graph-based clustering (shared nearest neighbors) on the unified cells-by-genes expression matrix and visualized our results via t-distributed stochastic neighbor embedding (t-SNE). Our unbiased analysis identified 6 unique macrophage clusters (Fig. 6C). Notably, there was similar representation within each macrophage cluster between the two models, with the exception of C5, which was predominantly comprised of macrophages from mice engrafted with DFBL-69487 and was dominated by genes associated with eosinophils (Supplementary Table 5). Importantly, two clusters (C2 and C4, respectively; Supplementary Fig. S6F; Supplementary Table S5) were enriched for macrophages from lymphoma-bearing mice treated with cyclophosphamide (Fig. 6C; $P = 3.7 \times 10^{-8}$ for C2, $P = 1.7 \times 10^{-9}$ for C4, Fisher exact test, Bonferroni corrected for 25 tests). Cells from clusters 2 and 4

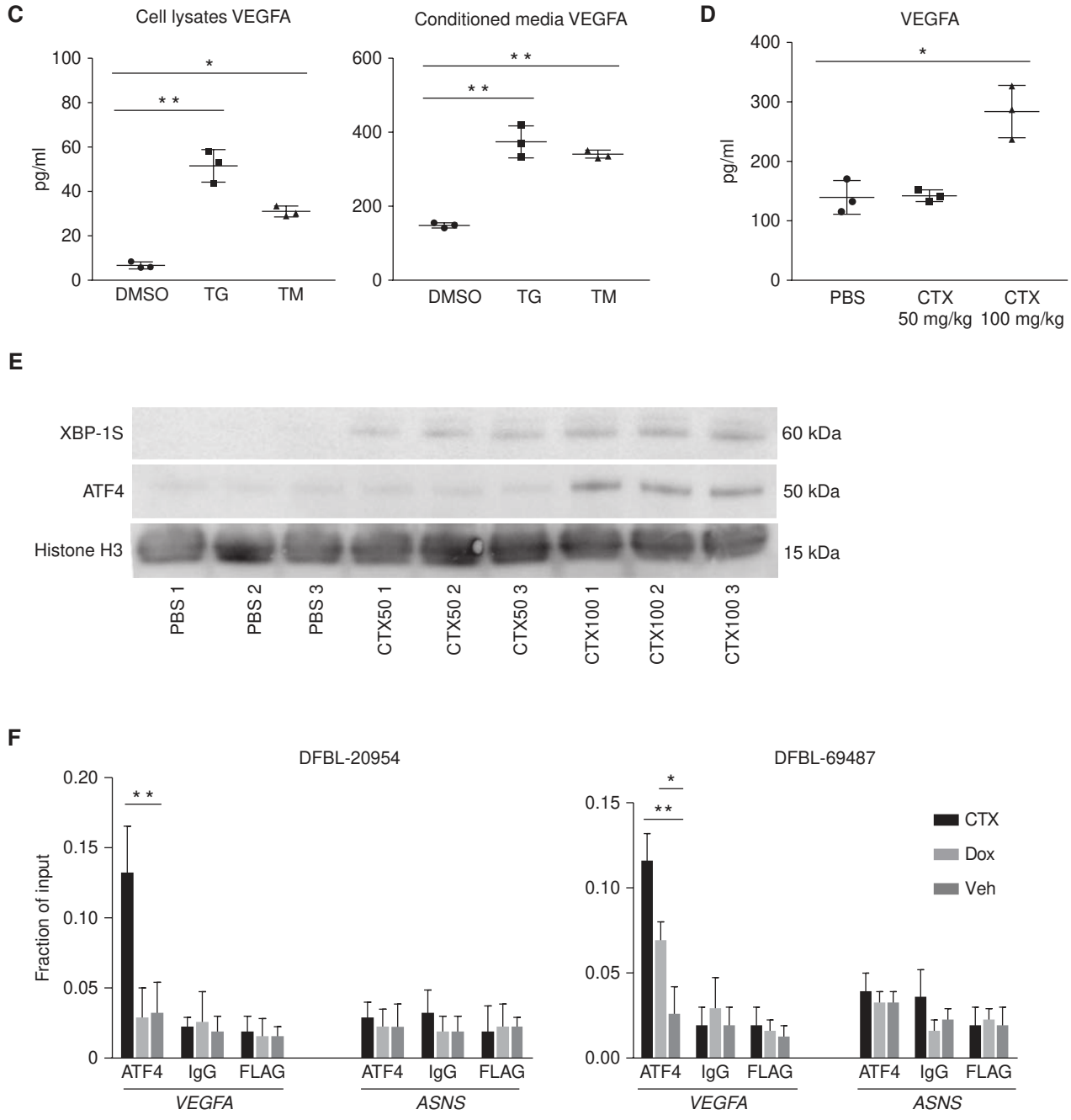

Figure 5. ***(Continued)*** **C,** Levels of human VEGFA in cells (left) or media (right) of DFBL-20954 cells isolated from BM and treated *ex vivo* for 24 hours with DMSO, thapsigargin (TG), or tunicamycin (TM). Two-sided Welch *t* test, *, $P < 0.05$; **, $P < 0.01$. **D,** Levels of human VEGFA from whole BM collected 16 hours after *in vivo* treatment of DFBL-20954–engrafted mice as indicated. Unpaired two-sided *t* test. **E,** Immunoblotting, as in **B**. **F,** ChIP-qPCR of ATF4 localization to exon 1 of human *VEGFA* or exon 7 of human *ASNS* in purified, viable BM DFBL-20954, and DFBL-69487 cells collected 16 and 48 hours, respectively, after treatment with vehicle, doxorubicin, or cyclophosphamide ($n = 3$ replicates per condition with multiple mice pooled for each replicate). Unpaired two-sided *t* test.

were enriched for expression of genes known to be important in macrophage-mediated phagocytosis, including CD36 and PPARγ (refs. 50, 51; Supplementary Tables S5 and S6).

We noted a striking increase in the expression of FCGR1, the high-affinity human IgG receptor, in cluster 2 macrophages (Fig. 6D; $P = 5.28 \times 10^{-15}$, Bonferroni corrected for 24 comparisons, effect size Cohen d = 1.04). At the same time, cluster 4 had markedly higher expression of FCGR4 (Fig. 6D; $P = 5.28 \times 10^{-15}$, Bonferroni corrected for 24 tests, effect size Cohen d = 2.54). Flow cytometric analysis of macrophages from the spleen and BM confirmed increases in the overall expression of activating Fc receptors (FCGR1, FCGR3, and FCGR4) and

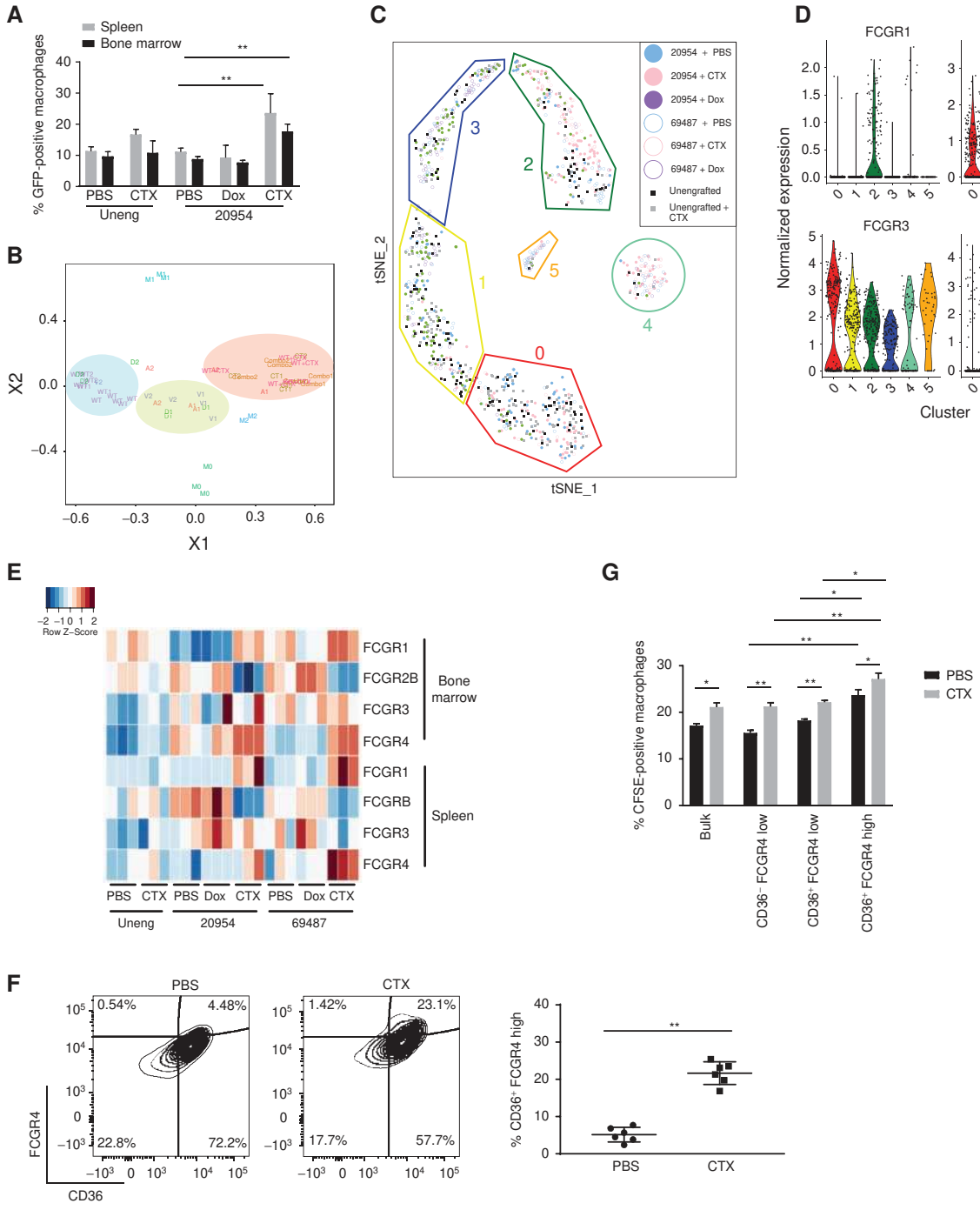

Figure 6. Cyclophosphamide induces super-phagocytic macrophages in lymphoma-engrafted bone marrow. **A,** Primary viable splenic (7AAD$^-$hCD19$^-$CD11b$^-$F4/80$^+$) and BM (7AAD$^-$hCD19$^-$CD11b$^+$F4/80$^+$) monocytes/macrophages were sorted from unengrafted or DFBL-20954–bearing NSG mice ($n = 3$ per condition) treated with PBS (Veh), doxorubicin (Dox), or cyclophosphamide (CTX) and cultured in the presence of GFP$^+$ Raji cells that were pretreated with alemtuzumab. Two-sided Welch *t* test, **, $P < 0.01$. **B,** MDS analysis of RNA-seq from BM macrophages comparing unengrafted (WT) or lymphoma-engrafted (DFBL-69487 = 1, DFBL-20954 = 2) mice treated with PBS (V), doxorubicin (D), cyclophosphamide (C), alemtuzumab (Alem), or cyclophosphamide + alemtuzumab (combo). Macrophages were harvested 48 hours after treatment. **C,** t-SNE plot of single-cell RNA-seq of BM macrophages from unengrafted (uneng) or engrafted mice treated with PBS, doxorubicin, or cyclophosphamide shows six clusters (left). Cluster 4 is enriched with macrophages from cyclophosphamide-treated, lymphoma-engrafted mice. Clusters and numbers in each cluster from each treatment group are indicated in the figure legend. **D,** Expression of Fc-gamma receptors from single-cell RNA-seq of sorted BM macrophages clustered as in **C**. **E,** Flow cytometric analysis of Fc-gamma receptor expression on macrophages from unengrafted or DFBL-29054–engrafted mice treated *in vivo* as indicated. Macrophages were collected 48 hours after treatment. Heat map represents Z-scores of MFIs normalized to isotype controls. **F,** Representative flow cytometry of BM macrophages collected from DFBL-29054–engrafted mice treated with PBS or cyclophosphamide. Unpaired two-sided *t* test. **G,** Macrophages from **F** were sorted as indicated or unsorted (Bulk), labeled with CFSE, and exposed to BM DFBL-20954 cells from mice treated with PBS or cyclophosphamide that were pretreated *ex vivo* with alemtuzumab ($n = 5$ mice per condition). Unpaired two-sided *t* test, *, $P < 0.05$; **, $P < 0.01$.

decreased expression of the inhibitory FCGR2B receptor on the surface of cells from lymphoma-engrafted mice treated with cyclophosphamide (Fig. 6E). Interestingly, doxorubicin treatment of lymphoma-engrafted mice increased FCGR2B surface expression on both splenic and BM macrophages (Fig. 6E). Ingenuity Pathway Analysis (IPA) of C2 and C4 cells showed enrichment of genes involved in Fc receptor–mediated phagocytosis and phagosome formation and maturation (Supplementary Tables S5 and S6).

For both lymphomas, we noted that cluster 4 macrophages comprised approximately 20% to 25% of BM macrophages after cyclophosphamide treatment. Thus, we hypothesized that cluster 4 specifically defines macrophages with "super-phagocytic" capacity for alemtuzumab-coated cells. To address this, we flow-sorted macrophages from the BM of lymphoma-bearing mice treated with vehicle or cyclophosphamide based on FCGR4 and CD36 (Fig. 6F). As expected, cyclophosphamide-treated mice had an increased percentage of BM FCGR4^{hi}/CD36^{+} macrophages (Fig. 6F). Phagocytosis of alemtuzumab-opsonized lymphoma cells was enhanced among macrophages from this population compared with CD36$^{lo/negative}$ or FCGR4^{lo} cells (Fig. 6G). Finally, IPA upstream pathway analysis showed VEGF as a regulator of the C4 signature (Supplementary Table S7). Thus, the cluster 4 signature defines a unique macrophage state that is induced specifically by cyclophosphamide in the presence of lymphoma cells and has enhanced ability to phagocytose antibody-coated lymphoma cells.

DISCUSSION

Treatment-resistant niches pose a challenge to effective cancer therapy. The bone marrow is a frequent site of minimal residual disease in both hematologic and nonhematologic tumors, suggesting compartment-specific mechanisms of resistance (52, 53). Using orthotopic models of aggressive human lymphoma, we recapitulated resistance to both antibody and doxorubicin therapy within the BM and defined resistance mechanisms through comparisons with the spleen, a site of consistent drug activity.

Previous analyses of antibody resistance in lymphomas have identified several lymphoma cell–autonomous mechanisms, including the loss of target antigen and changes in the expression of pro- and antiphagocytic factors (29, 54, 55). In our models, alemtuzumab resistance was achieved through BM remodeling that involved high lymphoma:macrophage ratios at later stages of engraftment. We recapitulated antibody resistance within the spleen solely by partial depletion of macrophages. Although clodronate may have unexpected effects on cells other than macrophages, these findings strongly suggest that lymphoma:macrophage ratio is a primary determinant of antibody response within our models. Late engraftment was associated with higher levels of CD32, galectin-1, and PGE2. Each of these factors can decrease antibody-mediated lymphoma clearance by macrophages (35–37), which we confirmed for both galectin-1 and PGE2. It remains poorly understood how the BM microenvironment interacts with lymphoma cells to modulate the expression of these factors as well as the extent to which other tumor types develop resistance within the BM through these same factors.

Treatment with high-dose cyclophosphamide (but not a dose closer to that in R-CHOP) overcame antibody resistance within the BM, leading to marked synergy with alemtuzumab. This suggests that diseases involving the BM that are known to be responsive to alemtuzumab, such as chronic lymphocytic leukemia, may benefit from combinations with high-dose cyclophosphamide. At the same time, other antibodies besides alemtuzumab presumably also synergize with high-dose cyclophosphamide if there is adequate expression of the target antigen. In fact, other studies have reported that cyclophosphamide can overcome resistance to rituximab or a carcinoma-specific antibody in an Fc receptor–dependent manner (20, 56). Notably, high doses of other alkylating agents also induced synergy within the BM to cyclophosphamide, but other classes of cytotoxic chemotherapy or navitoclax, which directly induces apoptosis, did not. Thus, the activity of high-dose alkylating agents does not solely involve either clastogenesis or apoptotic cell death. Instead, we show that cyclophosphamide treatment of engrafted mice leads to a remarkable infiltration of macrophages within the BM, an altered balance of pro- and antiphagocytic markers and secretion of prophagocytic cytokines.

A central unanswered question is whether the findings in the BM of our xenografts are applicable to sites with high tumor:effector cell ratios in humans. To this end, treatment with high-dose cyclophosphamide may be an effective strategy for overcoming sites of bulky disease, which are known to be relatively refractory to mAbs (18). Ultimately, paired biopsies from bulky and nonbulky sites of lymphoma will be needed to clarify whether the former have higher tumor:effector cell ratios and whether those ratios correlate with differential response to mAbs.

The antineoplastic activity of alkylating agents has classically been linked to the direct induction of DNA adducts that result in single- and double-strand DNA breaks (57). However, from the first description of these compounds it has been clear that they can alkylate a variety of proteins, lipids, and other molecules (58). On the basis of changes in gene expression induced by cyclophosphamide treatment, we identified ER stress within DHL cells after treatment with high-dose (but not lower-dose) cyclophosphamide. The mechanism through which high-dose cyclophosphamide induces this ER stress is unclear but it could involve protein misfolding, which is known to induce ER stress through the unfolded protein response (42). It is possible that chemical modifications of proteins and other non-DNA targets reach a threshold only with higher concentrations of alkylating agents and their metabolites. This would help explain why high-dose cyclophosphamide is required to induce ER stress. It also remains unclear to what extent ER stress is sufficient to drive the complex interactions between lymphoma cells and the BM microenvironment after cyclophosphamide treatment.

ER stress within BM lymphoma cells after cyclophosphamide treatment led to upregulation of ATF4, which can bind *VEGFA* regulatory regions. The associated secretory response, in concert with the more pro-phagocytic balance of lymphoma surface signals, then promotes macrophage phagocytosis. The VEGFA response is required, as either bevacizumab or SYK inhibition reversed the increased phagocytosis

induced by cyclophosphamide. These findings provide multiple notes of caution. Agents included within chemotherapy regimens such as glucocorticoids may suppress the activity of macrophages and thereby antagonize high-dose alkylating agents. Similarly, trials of bevacizumab or SYK inhibition, which both suppress macrophage-mediated clearance of lymphoma cells in our experiments, are currently under way in combinations with chemoimmunotherapy. It is possible that these agents will have direct cytotoxic effects on lymphoma cells but antagonize macrophage responses. Finally, studies using cell lines to identify interactions between therapeutic agents will not capture antagonisms that depend on microenvironmental and immune cell interactions.

Using single-cell RNA-seq, we show that a diverse set of transcriptionally unique macrophage clusters are present within lymphoma-engrafted BM, and this biology is markedly altered by cyclophosphamide. The classic distinctions between M0, M1, and M2 macrophages that were defined on the basis of *in vitro* studies fail to capture this diversity *in vivo* or the effects from cyclophosphamide. Most notably, cyclophosphamide treatment leads to marked enrichment of two unique macrophage subgroups, designated here as C2 and C4. C4 macrophages had high expression of FCGR4 and CD36 transcripts. Sorted macrophages with surface FCGR4^{hi}/CD36^{+} immunophenotype had "super-phagocytic" capacity when exposed to BM lymphoma cells *ex vivo*, suggesting that these are the primary effectors that mediate the activity of single-agent cyclophosphamide. In contrast, C2 macrophages were characterized by increased expression of FCGR1, the high-affinity Fc receptor that likely mediates most ADCP (59). Thus, one possibility is that C4 macrophages are capable of clearing lymphoma cells after cyclophosphamide treatment alone whereas C2 macrophages orchestrate most of the synergistic effects observed with the addition of alemtuzumab. It is also worth noting that doxorubicin treatment increased surface expression of the inhibitory FCGR2B on both splenic and BM macrophages (Fig. 6E), suggesting that combining doxorubicin with high-dose alkylating agents could suppress ADCP.

We opened a clinical trial of alemtuzumab plus cyclophosphamide in patients with CD52-positive lymphomas (https://clinicaltrials.gov/ct2/show/NCT03132584). Treatment with this dose of cyclophosphamide requires hospitalization, and patients receive alemtuzumab without steroids. Thus, the toxicity and cost are significant. It will be important to determine whether other agents that induce aspects of the "super-phagocytic" response we describe here are equally efficacious in model systems. These could include blockers of CD47–SIRPα interaction, direct inducers of ER stress, or agents that directly block mediators of antibody resistance within the BM such as nonsteroidal anti-inflammatory drugs to suppress PGE2 production. Strategies that avoid high doses of alkylating agents may have the additional advantage of maintaining aspects of adaptive immunity important for long-term tumor control and could be applied across multiple cancer types.

In summary, we describe a mechanism to sensitize treatment-refractory malignancies to immunotherapy that may be particularly relevant to tumors or specific tumor compartments that do not undergo rapid apoptosis in response to therapy. Current drug regimens include agents that may antagonize this process and thus subvert the efficacy of immune-directed therapies.

METHODS

Mouse Models and Therapeutics

DFBL-20954 and DFBL-69487 are available from the Public Repository of Xenografts (PRoXe; ref. 26). Six- to 8-week-old NSG mice (Jackson Labs) were injected with 10^6 tumor cells intravenously (i.v.). Mice were bled weekly and treatment was initiated when circulating disease was >2% as assessed by flow cytometry staining for hCD19 (clone HIB19, BioLegend) and hCD45 (clone HI30, Thermo Fisher Scientific). All blood samples were lysed with ammonium chloride red blood cell buffer (VWR) prior to staining.

Clinical-grade alemtuzumab (Genzyme-Sanofi) and rituximab (Roche) were obtained dissolved in PBS at 30 and 10 mg/mL, respectively, from the Dana-Farber Cancer Institute Pharmacy and Cologne. Prior to administration, alemtuzumab was diluted 1:30 in PBS (10 mg/kg doses) or 1:60 (5 mg/kg doses) and rituximab was diluted 1:5 and mice were dosed with 10 μL/g. Alemtuzumab was administered 5 mg/kg i.v. on day 0 and 5 mg/kg intraperitoneally (i.p.) on day 1 of treatment to avoid tumor-lysis syndrome, unless otherwise specified. Rituximab was given as a single dose at 20 mg/kg i.v. on day 0 of treatment. Alemtuzumab was conjugated with an APC Conjugation Kit (Abcam) as per the manufacturer's instructions.

Cyclophosphamide (Sigma Aldrich) was dissolved at 10 mg/mL in PBS and administered i.p. on day 0 at a dose of 10 μL/g of mouse body weight. For studies where cyclophosphamide was administered at 25 and 50 mg/kg, respectively, it was dissolved at 2.5 and 5 mg/mL PBS and dosed at 10 μL/g of mouse body weight. Doxorubicin (Tocris Bioscience) was dissolved at 0.5 mg/mL of 0.9% NaCl solution and administered intraperitoneally at 10 μL/g of mouse body weight. Ifosfamide (Sigma Aldrich) was dissolved at 20 mg/mL in PBS and administered as cyclophosphamide. Busulfan (Sigma Aldrich) was dissolved in DMSO and then in PBS to generate a 2.5 mg/mL solution with 10% DMSO and dosed as 10 μL/g mouse body weight for two days. Vincristine and prednisone were purchased from Sigma Aldrich and dissolved in PBS. R-CHOP dosing was given as follows: rituximab (20 mg/kg i.v., day 0), cyclophosphamide (30 mg/kg i.p., day 0), doxorubicin (2.58 mg/kg i.p., day 0), vincristine (0.38 mg/kg i.p., day 0), and prednisone (5 × 2 mg/kg i.p., starting on day 0). All drugs were given at 10 μL/g of mouse body weight. Bevacizumab was obtained from the Beth Israel Deaconess Medical Center pharmacy dissolved at 25 mg/mL in PBS and was administered at 25 mg/mL at 10 μL/g of mouse body weight on days −1, 0, and 1 of treatment. Navitoclax was dosed at 100 mg/kg orally on days 0–7. All *in vivo* experiments were conducted in accordance with Dana-Farber Cancer Institute Animal Care and Use Committee protocol #13-034.

BMDM Generation

Eight- to 10-week old NSG mice were euthanized and femurs were flushed with a 27G needle and sifted through a 70-μm filter. The filtrates were red blood cell (RBC) lysed with ammonium chloride (VWR) and plated in RPMI-1640 media supplemented with 10% L929 cultured cell media (ATCC), 10% FBS (Sigma Aldrich), and 1% penicillin/streptomycin solution (Thermo Fisher Scientific). Media were changed every 2–3 days until day 7 when the macrophages were used for functional assays.

Cell Culture

Raji-GFP cells were a generous gift from Dr. Izidore Lossos, and authenticity was validated by short tandem repeat profiling. Raji cells were maintained in RPMI-1640 media supplemented with 10% FBS

(Sigma Aldrich) and 1% penicillin/streptomycin solution (Thermo Fisher Scientific). Cells were split 1:10 every 2–3 days and checked for *Mycoplasma* every 3 months by the Universal Mycoplasma Detection Kit (ATCC) and were last checked on March 16, 2019.

Phagocytosis Assays (BMDM and In Vivo*–Derived Macrophages)*

In vitro–differentiated macrophages were generated as described above. On day 7, BMDMs were plated at 1×10^5 cells per well of a 24-well plate and serum-starved for 2 hours in RPMI-1640 media supplemented with 1% penicillin/streptomycin. Target tumor cells (3:1 tumor:macrophage ratio) were labeled with CFSE (CellTrace CFSE Cell Proliferation Kit, Thermo Fisher Scientific) as per the manufacturer's instructions, and 30 minutes prior to coincubation with macrophages were precoated with alemtuzumab, rituximab, or obinutuzumab (final concentration 20 μg/mL per ml of total culture media of total plates) at 37°C. Antibody-coated and uncoated tumor cells were then coincubated with macrophages for 2 hours. After incubation, wells were washed 2× with PBS and macrophages were detached by gentle scraping in ice-cold PBS. Cells were then preincubated with human (Human TruStain FcX, BioLegend) and murine Fc-Block (BD Biosciences) and then stained with CD11b (clone M1/M70, BioLegend) for 30 minutes at room temperature and analyzed using a Cytoflex (Beckman Coulter). Phagocytosis was measured as the fraction of GFP/CFSE–positive $CD11b^+$ macrophages. All cytokines used in the assays were purchased from PeproTech and added at the indicated doses immediately following the addition of tumor cells to the macrophage coculture. Recombinant human galectin-1 was purchased from R&D Systems. Prostaglandin E2 and BAY61-3606 were purchased from Sigma Aldrich. Mafosfamide and lactose were purchased from Santa Cruz Biotechnology.

For phagocytosis assays using *in vivo*–derived macrophages, 10^6 xenograft cells were injected into 6- to 10-week-old NSG mice. Once peripheral blood disease reached >2%, mice were treated with PBS, doxorubicin, or cyclophosphamide as described above. Age-controlled unengrafted mice were treated with PBS or cyclophosphamide as above. Mice were euthanized and bone marrow and spleens were processed as described above. Samples were pretreated with human Fc-block and stained with 7-AAD (Thermo Fisher Scientific), human CD19 (clone HIB19, BioLegend), murine CD11b (clone M1/M70, BioLegend), and F4/80 (clone BM8, BD Biosciences) antibodies and sorted using a BD FACSAria II (BD Biosciences). Splenic macrophages were defined as $7AAD^-CD19^-CD11b^-F4/80^+$ cells, and BM macrophages were defined as $7AAD^-CD19^-CD11b^+F4/80^+$ cells. Cells were plated at 50,000 cells per well in a 96-well plate in RPMI-1640 media supplemented with 10% L929 media, 10% FBS, 1% penicillin/streptomycin and 50 mmol/L 2-ME (Sigma Aldrich). Once cells attached and spinous processes were microscopically visible (12–16 hours after plating), macrophages were serum-starved for 2 hours and cocultured with CFSE-stained tumor cells ± alemtuzumab as described above. Cells were processed and analyzed as above but murine F4/80 was used to label macrophages instead of CD11b. Phagocytosis was measured as the fraction of GFP/CFSE–positive $F4/80^+$ cells.

Cytokine Arrays

Mouse tibias were flushed. Whole-cell suspensions or pelleted cells and the corresponding aqueous portions were incubated with NP-40 lysis buffer with Halt protease and phosphatase inhibitors 100× (Life Technologies). Thapsigargin and tunicamycin were purchased from Cell Signaling Technology and dosed at 2,000 nmol/L and 10 μg/mL, respectively. Protein amounts were quantified with a Pierce BCA Protein Assay Kit (Life Technologies). Samples were diluted to contain equal amounts of total protein and were submitted to Eve Technologies for Human 65-plex and Murine-41 plex discovery arrays.

ELISA

Femurs were flushed and mouse depleted as described above. Protein amount was quantified using a Pierce BCA Protein Assay Kit (Life Technologies). Human galectin-1 ELISA Kit (R&D Systems) was from Thermo Fisher Scientific. Prostaglandin E2 ELISA Kit was purchased from Abcam. Standard curves were generated from provided reagents and from recombinant proteins and quantified using SoftMax Pro software on a Spectromax M190 per the manufacturer's instructions.

Conditioned Media Generation

NSG mice were injected and treated as above. Six hours after treatment, human tumor cells were purified using an EasySep Mouse/Human Chimera Isolation Kit (StemCell Technologies). Purified, pooled cells (10^7) were cultured in 10 mL of X-Vivo 15 media (Lonza Bioscience) for 24 hours post-isolation. Cells were pelleted with centrifugation ($500 \times g$) for 10 minutes and supernatant removed and applied to macrophages following serum starvation for phagocytosis assays. Thapsigargin- and tunicamycin-conditioned media were generated from 10^6 cells.

Statistical Analysis

Overall survival was determined by the Kaplan–Meier method using the log-rank test and considered significant at the <0.05 level. Alemtuzumab and cyclophosphamide synergy was calculated as described previously (20). Comparisons of continuous measures between two groups was made using a two-sided Welch t test and were considered significant at the 0.05 level. Differential expression of bulk RNA-seq between experimental conditions was determined using raw count data and normalization procedures within the DESeq2 package in R based on a negative binomial distribution. The false discovery rate (FDR) by Benjamini and Hochberg method was used to adjust for multiple comparisons. Ordered lists determined by differential expression analysis were then used in GSEA using tools developed by the Broad Institute, and FDR q values were also reported.

Disclosure of Potential Conflicts of Interest

C.P. Pallasch reports receiving commercial research grants from Gilead Sciences and Genzyme and has received speakers bureau honoraria from Gilead Sciences and Roche. J.C. Aster is a consultant/advisory board member for Ayala, Cellestia, and Epizyme. No potential conflicts of interest were disclosed by the other authors.

Authors' Contributions

Conception and design: C.P. Pallasch, M.T. Hemann, D.M. Weinstock
Development of methodology: C. Lossos, Y. Liu, A.L. Christie, C.P. Pallasch, Q.-D. Nguyen, J.C. Aster, A.K. Shalek, D.M. Weinstock
Acquisition of data (provided animals, acquired and managed patients, provided facilities, etc.): C. Lossos, Y. Liu, K.E. Kolb, A.L. Christie, A. van Scoyk, S.M. Prakadan, K. Shigemori, S. Morrow, O.D. Plana, C. Fraser, K.L. Jones, H. Liu, R. Modiste, Q.-D. Nguyen, J.W. Craig, J.C. Aster, K.A. Sarosiek
Analysis and interpretation of data (e.g., statistical analysis, biostatistics, computational analysis): C. Lossos, Y. Liu, K.E. Kolb, A.L. Christie, S.M. Prakadan, K.E. Stevenson, Q.-D. Nguyen, E.A. Morgan, F. Vega, K.A. Sarosiek, A.K. Shalek, M.T. Hemann, D.M. Weinstock
Writing, review, and/or revision of the manuscript: C. Lossos, Y. Liu, K.E. Kolb, S.M. Prakadan, K.E. Stevenson, J.W. Craig, E.A. Morgan, K.A. Sarosiek, A.K. Shalek, D.M. Weinstock
Administrative, technical, or material support (i.e., reporting or organizing data, constructing databases): Y. Liu, K.E. Stevenson, C.P. Pallasch
Study supervision: A.K. Shalek, D.M. Weinstock

Acknowledgments

We thank the Dana-Farber Hematologic Neoplasia Flow Cytometry Core for their assistance. We also thank Drs. Anthony Letai, Roberto Chiarle, and Andrew Lane for thoughtful discussions and experimental suggestions. Thank you to Dr. Izidore Lossos for a critical reading of the manuscript. The project described was supported by award number T32GM007753 (C. Lossos) from the National Institute of General Medical Sciences, the Cancer Systems Biology Consortium U54 CA217377 (A.K. Shalek), the Searle Scholars Program (A.K. Shalek), the Beckman Young Investigator Program (A.K. Shalek), NIH New Innovator Award 1DP2OD020839 (A.K. Shalek), NIH 5U24AI118672 (A.K. Shalek), NIH 1R33CA202820 (A.K. Shalek), NIH 2U19AI089992 (A.K. Shalek), NIH 1R01HL134539 (A.K. Shalek), NIH 2RM1HG006193 (A.K. Shalek), 2P01AI039671 (A.K. Shalek), the Pew-Stewart Scholars (A.K. Shalek), a Sloan Fellowship in Chemistry (A.K. Shalek), and partially by Cancer Center Support (core) Grant P30-CA14051 from the National Cancer Institute (A.K. Shalek), the Center for Precision Cancer Medicine at MIT (Y. Liu and M.T. Hemann), and the Dana-Farber/Koch Institute Bridge Project (M.T. Hemann and D.M. Weinstock). The content is solely the responsibility of the authors and does not necessarily represent the official views of the National Institute of General Medical Sciences or the National Institutes of Health.

The costs of publication of this article were defrayed in part by the payment of page charges. This article must therefore be hereby marked *advertisement* in accordance with 18 U.S.C. Section 1734 solely to indicate this fact.

Received November 27, 2018; revised March 28, 2019; accepted April 25, 2019; published first April 30, 2019.

REFERENCES

1. George P. Haemorrhagic cystitis and cyclophosphamide. Lancet 1963; 2:942.
2. Solomon J, Alexander MJ, Steinfeld JL. Cyclophosphamide. A clinical study. JAMA 1963;183:165–70.
3. Burkitt D. Long-term remissions following one and two-dose chemotherapy for African lymphoma. Cancer 1967;20:756–9.
4. Clifford P, Singh S, Stjernsward J, Klein G. Long-term survival of patients with Burkitt's lymphoma: an assessment of treatment and other factors which may relate to survival. Cancer Res 1967;27:2578–615.
5. Frei E 3rd, Cucchi CA, Rosowsky A, Tantravahi R, Bernal S, Ervin TJ, et al. Alkylating agent resistance: in vitro studies with human cell lines. Proc Nat Acad Sci U S A 1985;82:2158–62.
6. Tsuruo T, Iida H, Tsukagoshi S, Sakurai Y. Potentiation of vincristine and Adriamycin effects in human hemopoietic tumor cell lines by calcium antagonists and calmodulin inhibitors. Cancer Res 1983;43:2267–72.
7. Yang W, Soares J, Greninger P, Edelman EJ, Lightfoot H, Forbes S, et al. Genomics of drug sensitivity in cancer (GDSC): a resource for therapeutic biomarker discovery in cancer cells. Nucleic Acids Res 2013;41:D955–61.
8. Saida Y, Watanabe S, Tanaka T, Baba J, Sato K, Shoji S, et al. Critical roles of chemoresistant effector and regulatory T cells in antitumor immunity after lymphodepleting chemotherapy. J Immunol 2015; 195:726–35.
9. Miller JS, Weisdorf DJ, Burns LJ, Slungaard A, Wagner JE, Verneris MR, et al. Lymphodepletion followed by donor lymphocyte infusion (DLI) causes significantly more acute graft-versus-host disease than DLI alone. Blood 2007;110:2761–3.
10. Wang YJ, Fletcher R, Yu J, Zhang L. Immunogenic effects of chemotherapy-induced tumor cell death. Genes Dis 2018;5:194–203.
11. Mantovani A, Polentarutti N, Luini W, Peri G, Spreafico F. Role of host defense merchanisms in the antitumor activity of adriamycin and daunomycin in mice. J Natl Cancer Inst 1979;63:61–6.
12. Ferry JA. Burkitt's lymphoma: clinicopathologic features and differential diagnosis. Oncologist 2006;11:375–83.
13. Ford CA, Petrova S, Pound JD, Voss JJ, Melville L, Paterson M, et al. Oncogenic properties of apoptotic tumor cells in aggressive B cell lymphoma. Curr Biol 2015;25:577–88.
14. Weiner GJ. Rituximab: mechanism of action. Semin Hematol 2010; 47:115–23.
15. Leidi M, Gotti E, Bologna L, Miranda E, Rimoldi M, Sica A, et al. M2 macrophages phagocytose rituximab-opsonized leukemic targets more efficiently than m1 cells in vitro. J Immunol 2009;182:4415–22.
16. Weiskopf K, Weissman IL.Macrophages are critical effectors of antibody therapies for cancer. MAbs 2015;7:303–10.
17. McLaughlin P, Grillo-Lopez AJ, Link BK, Levy R, Czuczman MS, Williams ME, et al. Rituximab chimeric anti-CD20 monoclonal antibody therapy for relapsed indolent lymphoma: half of patients respond to a four-dose treatment program. J Clin Oncol 1998;16:2825–33.
18. Lundin J, Osterborg A, Brittinger G, Crowther D, Dombret H, Engert A, et al. CAMPATH-1H monoclonal antibody in therapy for previously treated low-grade non-Hodgkin's lymphomas: a phase II multicenter study. European Study Group of CAMPATH-1H Treatment in Low-Grade Non-Hodgkin's Lymphoma. J Clin Oncol 1998;16: 3257–63.
19. Leskov I, Pallasch CP, Drake A, Iliopoulou BP, Souza A, Shen CH, et al. Rapid generation of human B-cell lymphomas via combined expression of Myc and Bcl2 and their use as a preclinical model for biological therapies. Oncogene 2013;32:1066–72.
20. Pallasch CP, Leskov I, Braun CJ, Vorholt D, Drake A, Soto-Feliciano YM, et al. Sensitizing protective tumor microenvironments to antibody-mediated therapy. Cell 2014;156:590–602.
21. Craig JW, Mina MJ, Crombie JL, LaCasce AS, Weinstock DM, Pinkus GS, et al. Assessment of CD52 expression in "double-hit" and "double-expressor" lymphomas: Implications for clinical trial eligibility. PLoS One 2018;13:e0199708.
22. Yao Z, Deng L, Xu-Monette ZY, Manyam GC, Jain P, Tzankov A, et al. Concordant bone marrow involvement of diffuse large B-cell lymphoma represents a distinct clinical and biological entity in the era of immunotherapy. Leukemia 2018;32:353–63.
23. Khelfa Y, Lebowicz Y, Jamil MO. Double-hit large B cell lymphoma. Curr Oncol Rep 2017;19:74.
24. Burotto M, Berkovits A, Dunleavy K. Double hit lymphoma: from biology to therapeutic implications. Expert Rev Hematol 2016;9: 669–78.
25. Teo EC, Chew Y, Phipps C. A review of monoclonal antibody therapies in lymphoma. Crit Rev Oncol Hematol 2016;97:72–84.
26. Townsend EC, Murakami MA, Christodoulou A, Christie AL, Koster J, DeSouza TA, et al. The public repository of xenografts enables discovery and randomized phase II-like trials in mice. Cancer Cell 2016;29:574–86.
27. Wu D, Wood BL, Dorer R, Fromm JR. "Double-Hit" mature B-cell lymphomas show a common immunophenotype by flow cytometry that includes decreased CD20 expression. Am J Clin Pathol 2010;134: 258–65.
28. Harrington AM, Olteanu H, Kroft SH, Eshoa C. The unique immunophenotype of double-hit lymphomas. Am J Clin Pathol 2011; 135:649–50.
29. Beers SA, French RR, Chan HT, Lim SH, Jarrett TC, Vidal RM, et al. Antigenic modulation limits the efficacy of anti-CD20 antibodies: implications for antibody selection. Blood 2010;115:5191–201.
30. Koch R, Christie AL, Crombie JL, Palmer AC, Plana D, Shigemori K, et al. Biomarker-driven strategy for MCL1 inhibition in T-cell lymphomas. Blood 2018;133:566–75.
31. Matthews JM, Bhatt S, Patricelli MP, Nomanbhoy TK, Jiang X, Natkunam Y, et al. Pathophysiological significance and therapeutic targeting of germinal center kinase in diffuse large B-cell lymphoma. Blood 2016;128:239–48.
32. Ni Chonghaile T, Sarosiek KA, Vo TT, Ryan JA, Tammareddi A, Moore Vdel G, et al. Pretreatment mitochondrial priming correlates with clinical response to cytotoxic chemotherapy. Science 2011;334: 1129–33.

33. Morris EC, Rebello P, Thomson KJ, Peggs KS, Kyriakou C, Goldstone AH, et al. Pharmacokinetics of alemtuzumab used for in vivo and in vitro T-cell depletion in allogeneic transplantations: relevance for early adoptive immunotherapy and infectious complications. Blood 2003;102:404–6.
34. Hu Y, Shields J, Rao S, Lamorte M, Woodworth L, Kennedy B, et al. Alemtuzumab activity and CD52 expression in human CD52 transgenic mice [abstract]. In: Proceedings of the 98th AACR Annual Meeting; Apr 14–18; Los Angeles, CA: Philadelphia (PA): AACR; 2007. Abstract nr 4133.
35. Aronoff DM, Canetti C, Peters-Golden M. Prostaglandin E2 inhibits alveolar macrophage phagocytosis through an E-prostanoid 2 receptor-mediated increase in intracellular cyclic AMP. J Immunol 2004;173:559–65.
36. Lim SH, Vaughan AT, Ashton-Key M, Williams EL, Dixon SV, Chan HT, et al. Fc gamma receptor IIb on target B cells promotes rituximab internalization and reduces clinical efficacy. Blood 2011;118:2530–40.
37. Lykken JM, Horikawa M, Minard-Colin V, Kamata M, Miyagaki T, Poe JC, et al. Galectin-1 drives lymphoma CD20 immunotherapy resistance: validation of a preclinical system to identify resistance mechanisms. Blood 2016;127:1886–95.
38. Yoon KW, Byun S, Kwon E, Hwang SY, Chu K, Hiraki M, et al. Control of signaling-mediated clearance of apoptotic cells by the tumor suppressor p53. Science 2015;349:1261669.
39. Center DM, Cruikshank W. Modulation of lymphocyte migration by human lymphokines. I. Identification and characterization of chemoattractant activity for lymphocytes from mitogen-stimulated mononuclear cells. J Immunol 1982;128:2563–8.
40. Yang M, Shao JH, Miao YJ, Cui W, Qi YF, Han JH, et al. Tumor cell-activated CARD9 signaling contributes to metastasis-associated macrophage polarization. Cell Death Differ 2014;21:1290–302.
41. Ye J, Kumanova M, Hart LS, Sloane K, Zhang H, De Panis DN, et al. The GCN2-ATF4 pathway is critical for tumour cell survival and proliferation in response to nutrient deprivation. EMBO J 2010;29:2082–96.
42. Ghosh R, Lipson KL, Sargent KE, Mercurio AM, Hunt JS, Ron D, et al. Transcriptional regulation of VEGF-A by the unfolded protein response pathway. PLoS One 2010;5:e9575.
43. Binet F, Sapieha P. ER stress and angiogenesis. Cell Metab 2015; 22:560–75.
44. Schmitz ML, Shaban MS, Albert BV, Gokcen A, Kracht M. The crosstalk of endoplasmic reticulum (ER) stress pathways with NF-κB: complex mechanisms relevant for cancer, inflammation and infection. Biomedicines 2018;6:58.
45. Tam AB, Mercado EL, Hoffmann A, Niwa M. ER stress activates NF-kappaB by integrating functions of basal IKK activity, IRE1 and PERK. PLoS One 2012;7:e45078.
46. Oskolkova OV, Afonyushkin T, Leitner A, von Schlieffen E, Gargalovic PS, Lusis AJ, et al. ATF4-dependent transcription is a key mechanism in VEGF up-regulation by oxidized phospholipids: critical role of oxidized sn-2 residues in activation of unfolded protein response. Blood 2008;112:330–9.
47. Pereira ER, Frudd K, Awad W, Hendershot LM. Endoplasmic reticulum (ER) stress and hypoxia response pathways interact to potentiate hypoxia-inducible factor 1 (HIF-1) transcriptional activity on targets like vascular endothelial growth factor (VEGF). J Biol Chem 2014;289:3352–64.
48. Jablonski KA, Amici SA, Webb LM, Ruiz-Rosado Jde D, Popovich PG, Partida-Sanchez S, et al. Novel markers to delineate murine M1 and M2 macrophages. PLoS One 2015;10:e0145342.
49. Picelli S, Bjorklund AK, Faridani OR, Sagasser S, Winberg G, Sandberg R. Smart-seq2 for sensitive full-length transcriptome profiling in single cells. Nat Methods 2013;10:1096–8.
50. A-Gonzalez N, Quintana JA, Garcia-Silva S, Mazariegos M, Gonzalez de la Aleja A, Nicolas-Avila JA, et al. Phagocytosis imprints heterogeneity in tissue-resident macrophages. J Exp Med 2017;214:1281–96.
51. Fadok VA, Warner ML, Bratton DL, Henson PM. CD36 is required for phagocytosis of apoptotic cells by human macrophages that use either a phosphatidylserine receptor or the vitronectin receptor (alpha v beta 3). J Immunol 1998;161:6250–7.
52. Campana D. Minimal residual disease in acute lymphoblastic leukemia. Hematol Am Soc Hematol Educ Program 2010;2010:7–12.
53. Ignatiadis M, Reinholz M. Minimal residual disease and circulating tumor cells in breast cancer. Breast Cancer Res 2011;13:222.
54. Roghanian A, Teige I, Martensson L, Cox KL, Kovacek M, Ljungars A, et al. Antagonistic human FcgammaRIIB (CD32B) antibodies have anti-tumor activity and overcome resistance to antibody therapy in vivo. Cancer Cell 2015;27:473–88.
55. Dahal LN, Dou L, Hussain K, Liu R, Earley A, Cox KL, et al. STING activation reverses lymphoma-mediated resistance to antibody immunotherapy. Cancer Res 2017;77:3619–31.
56. Hubert P, Heitzmann A, Viel S, Nicolas A, Sastre-Garau X, Oppezzo P, et al. Antibody-dependent cell cytotoxicity synapses form in mice during tumor-specific antibody immunotherapy. Cancer Res 2011; 71:5134–43.
57. Zhou GH, Teicher BA, Frei E 3rd. Postlabeling detection of DNA adducts of antitumor alkylating agents. Cancer Chemother Pharmacol 1996;38:71–80.
58. Warwick GP. The mechanism of action of alkylating agents. Cancer Res 1963;23:1315–33.
59. Overdijk MB, Verploegen S, Ortiz Buijsse A, Vink T, Leusen JH, Bleeker WK, et al. Crosstalk between human IgG isotypes and murine effector cells. J Immunol 2012;189:3430–8.